Fuel Processing Technology 152 (2016) 156–175

Contents lists available at ScienceDirect

Fuel Processing Technology

journal homepage: www.elsevier.com/locate/fuproc

Research article

Comparative study of Ni, Co, Cu supported on γ-alumina catalysts for hydrogen production via the glycerol steam reforming reaction

Kiriakos N. Papageridis [a], Giorgos Siakavelas [a,b], Nikolaos D. Charisiou [a], Dimitrios G. Avraam [a,c], Lazaros Tzounis [d], Kaliopi Kousi [e], Maria A. Goula [a,b,*]

[a] Laboratory of Alternative Fuels and Environmental Catalysis, Department of Environmental and Pollution Control Engineering, School of Applied Sciences, Technological Education Institution of Western Macedonia (TEIWM), GR-50100, Koila, Kozani, Greece
[b] School of Science and Technology, Hellenic Open University, Tsamadou 13–15, GR-26222 Patras, Greece
[c] Department of Environment and Hydroeconomy, Regional Unity of Imathia, Region of Central Macedonia, GR-59131 Veria, Greece
[d] Laboratory for Thin Films-Nanosystems and Nanometrology (LTFN), Department of Physics, Aristotle University of Thessaloniki, GR-54124 Thessaloniki, Greece
[e] Department of Chemistry, University of Patras, GR-26504 Patras, Greece

ARTICLE INFO

Article history:
Received 23 December 2015
Received in revised form 27 May 2016
Accepted 18 June 2016
Available online 4 July 2016

Keywords:
Hydrogen production
Glycerol steam reforming
Nickel
Cobalt
Copper
Alumina

ABSTRACT

Catalysts with active phase Ni, Co or Cu supported on γ-alumina were synthesized at constant loading (8 wt.%) and tested for the glycerol steam reforming reaction (GSR). The synthesized samples, at their calcined and/or their reduced form, were characterized by BET, ICP, XRD, DRS, NH_3-TPD, CO_2-TPD, TPR and SEM. The carbon deposited on their surface under reaction conditions was characterized by TEM, TPO, TGA and Raman. Catalytic performance for the glycerol steam reforming reaction was studied in order to investigate the effects of reaction temperature on: (i) glycerol total conversion, (ii) glycerol conversion to gaseous products, (iii) hydrogen selectivity and yield, (iv) selectivity of carbonaceous gaseous products, (v) selectivity of liquid products and (vi) molar ratios of H_2/CO and CO/CO_2 in the gaseous products' mixture. The stability of all catalysts was also investigated through time on stream experiments. It was concluded that catalytic performance, including liquid products' distribution, depends on the acid-base properties of the materials. Specifically, a drastic drop in the activity of the Ni/Al catalyst was observed, while Co/Al and Cu/Al catalysts deactivate in a slower rate, confirming that coke deposition, associated with dehydration, cracking and polymerization reactions, takes place on the catalyst's surface strong acid sites.

1. Introduction

The issues emanating from the use of fossil fuels are widely known. They relate to the finite nature of these resources (which in turn raises questions regarding affordability, accessibility, security of supply and competition among state sponsored actors), and the effects that 'greenhouse gases' are having on the planet's climate [1–5]. In the transport sector, where the fuels currently used are almost entirely based on non-renewable sources, a possible solution may be provided by biofuels, i.e., fuels that are ultimately derived from biomass sources and can thus be considered carbon neutral [6–10]. Due to, a large part, the policies adopted by the European Union, biodiesel production increased by 3000% between 2000 and 2012 [11–13].

Biodiesel is currently produced from the transesterification reaction between vegetable oils or animal fats and principally methanol in the presence of an acidic or alkaline catalyst to form the biodiesel; fatty acid methyl esters (FAME) or fatty acid ethyl esters (FAEE), as shown in Eq. (1):

$$\underset{\text{Glycerides}}{C_3H_5\,(OOC)_3\,(R_n)_3} + \underset{\text{Alcohols}}{3R\prime OH} \leftrightarrow \underset{\text{Esters}}{3R_nCOOR\prime} + \underset{\text{Glycerol}}{C_3H_5(OH)_3} \qquad (1)$$

The principal byproduct of the biodiesel industry is glycerol, as every 100 g of oil undergoing the transesterification process produces 10 g of glycerol as byproduct [14–17]. Glycerol can be used for the production of hydrogen, a clean energy source whose demand is expected to greatly increase in the future, mainly due to technological advancements in the fuel cell industry [18–20]. Hydrogen can be produced from glycerol by catalytic reactions such as, steam reforming (GSR) [e.g. 21–24], oxidative steam reforming (OSR) [25–28], auto-thermal reforming (ATR) [29–32], aqueous phase reforming (APR) [33–36], and supercritical water (SCW) reforming [37–39].

GSR is attractive because, as can be deduced from Eq. (2), every mole of glycerol fed to the reactor can theoretically produce seven moles of hydrogen. In essence, Eq. (2) may be viewed as the combination of

---

* Corresponding author at: Department of Environmental and Pollution Control Engineering, School of Applied Sciences, Technological Education Institution of Western Macedonia (TEIWM), GR-50100, Koila, Kozani, Greece.
E-mail address: mgoula@teiwm.gr (M.A. Goula).

http://dx.doi.org/10.1016/j.fuproc.2016.06.024
0378-3820/

glycerol decomposition (Eq. (3)) and water-gas shift reactions (Eq. (4)). However, these reactions may also be accompanied by methanation (Eq. (5)), methane dry reforming (Eq. (6)), methane steam reforming (Eq. (7)) and a series of reactions for carbon formation (Eqs. (8)–(11)) that depend on the operating conditions; thus, it is justifiable to say that the GSR is a fairly complex process [40–43].

$$C_3H_8O_3(g)+3H_2O(g)\rightarrow 3CO_2(g)+7H_2(g) \quad (\Delta H^o = 123 \text{ kJ/mole}) \tag{2}$$

$$C_3H_8O_3(g)\rightarrow 3CO(g)+4H_2(g) \quad (\Delta H^o = 245 \text{ kJ/mole}) \tag{3}$$

$$CO(g)+H_2O(g)\leftrightarrow CO_2(g)+H_2(g) \quad (\Delta H^o = -41 \text{ kJ/mole}) \tag{4}$$

$$CO_2(g)+4H_2(g)\leftrightarrow CH_4(g)+2H_2O(g) \quad (\Delta H^o = -165 \text{ kJ/mole}) \tag{5}$$

$$CH_4(g)+CO_2(g)\rightarrow 2H_2(g)+2CO(g) \quad (\Delta H^o = 247 \text{ kJ/mole}) \tag{6}$$

$$CH_4(g)+H_2O(g)\leftrightarrow 3H_2(g)+CO(g) \quad (\Delta H^o = -206 \text{ kJ/mole}) \tag{7}$$

$$2CO(g)\leftrightarrow CO_2(g)+C(s) \quad (\Delta H^o = 172 \text{ kJ/mole}) \tag{8}$$

$$CH_4(g)\rightarrow 2H_2(g)+C(s) \quad (\Delta H^o = 75.6 \text{ kJ/mole}) \tag{9}$$

$$CO(g)+H_2(s)\rightarrow H_2O(g)+C(s) \quad (\Delta H^o = 131 \text{ kJ/mole}) \tag{10}$$

$$C_3H_8O_3(g)\rightarrow H_2(g)+3H_2O(g)+3C(s) \tag{11}$$

Thermodynamic studies have mainly explored the non-stochiometric approach, which is based on the minimization of Gibbs free energy as a function of temperature, pressure and species molar numbers [44–47]. Its advantage over the stochiometric approach lies with the fact that it does not require a selection of the possible set of reactions, no divergence occurs during the computation and it is not necessary to provide an accurate estimation of the initial equilibrium composition [48]. In brief, thermodynamics predict that the production of H_2 is strongly influenced by the reaction temperature and the water to glycerol feed ratio (WGFR). Given that the GSR is a strongly endothermic process ($\Delta H^0 > 0$), higher temperatures result in the production of higher amounts of hydrogen, while at lower temperatures, the production of CO_2 and CH_4 is favored. The latter is usually attributed to the water gas shift and methanation reactions, as both are exothermic and are thus more likely to occur at low temperatures. The production of CO, which is also favored at high temperatures, is usually attributed to the reverse water gas shift (RWGS) reaction. Regarding the effects of WGFR, it is generally accepted that excess water results in the production of more hydrogen following the Le Chatelier principle. However, it has been reported that when the WGFR exceeds 12 the H_2 production increases at slow rates. In summary, it has been suggested that the ideal condition to obtain H_2 is at temperatures between 600 and 700 °C and molar ratio of water to glycerol from 9:1 to 12:1. Under these conditions, methane production is minimized and carbon formation is thermodynamically inhibited [19,44–48].

For the glycerol steam reforming reaction, the catalyst influences the steps involved in the cleavage of C—C, O—H and C—H bonds of the glycerol molecule, and the maintenance of the C—O ones [49,50]. Studies reporting the performance of different catalytic systems for the GSR have investigated monometallic or bimetallic systems based on unmodified and/or modified supports. Considerable attention has been devoted to systems that are based on noble metals, namely Platinum (Pt) [20,23,49,51–55], Ruthenium (Ru) [20,56–58], Rhodium (Rh) [20,59], Iridium (Ir) [20,60] and Palladium (Pd) [20] or bimetallic systems that combine noble and transition metals [23,51,56,61–64]. Although noble metal based catalysts are usually more active and more stable during GSR, their high cost virtually prohibits their use on an industrial scale [19,40,41]. Thus, considerable efforts have been devoted at developing catalysts based on transition metals, with Nickel (Ni) attracting the lion's share of researchers attention [20–23,43,51,59–61,65–93]. A few researchers have also tested catalysts with Cobalt (Co) as the active phase, in both monometalic [60,64,82,89,94] and bimetallic systems, usually in combination with Ni [74], Rh [63,64,82] or Ru [62]. Copper (Cu), to the best of our knowledge, has only been used in bimetallic systems, and only in combination with Ni [24,77,83].

The reasons that Ni-based systems have attracted so much of researchers' interest are twofold; on one hand, such catalysts have lower cost and higher availability than noble metal catalysts, and on the other hand, Ni-based catalysts have good intrinsic activity, especially if the Ni is highly dispersed over the support [71,76]. An additional factor that enhances the appeal of Ni catalysts is that they are already widely used in the petroleum and natural gas processing industries [95,96]. However, there are two main issues associated with such catalysts. Firstly, it has been reported that Ni-based systems suffer from deactivation due to carbon formation, as the carbon tends to deposit and cover the active sites of the catalyst's surface. Secondly, they suffer from metal particles sintering, due to a lack of adequate thermal stability [24,51,77,78].

The effort to improve catalyst's stability and activity has also led researchers to investigate a variety of metal oxides as supports and/or promoters, e.g. MgO, CaO, Al_2O_3, SiO_2, ZrO_2, CeO_2, La_2O_3, TiO_2 and Y_2O_3; with alumina attracting considerable interest due to its high specific surface area (which is responsible for improved metal dispersion) and mechanical and chemical resistance under reaction conditions [77,97,98]. However, it is also known that carbon deposition and catalyst sintering, both factors that result in the de-activation of the catalyst, are also promoted when alumina is used as support. The reactions that are responsible for carbon formation are those associated with dehydration, cracking and polymerization. Catalyst sintering is thought to occur during the transition of alumina to crystalline phase during reaction [23,79,99,100].

As in the present study we compare alumina supported Ni, Co and Cu catalysts, we deemed it necessary to provide a short overview of selected works that have investigated similar systems, i.e., monometallic Ni, and Co systems based solely on alumina (Table 1). Cheng et al. [22], investigated a Ni/Al (15 wt.% Ni) catalyst at temperatures in the range 450–550 °C using a glycerol–water mixture containing 30–60 wt.% glycerol, only analyzing the gaseous products of the reaction. They reported production of 2.6–4.8 mol of hydrogen/mol of glycerol (i.e. significantly lower than that predicted by thermodynamics) and concluded that carbon deposition was significant at 550 °C, even under excess steam conditions. Interestingly, the authors reported an overall glycerol conversion value of ≈80% at high temperatures. In a separate work, Cheng et al., investigated a Co/Al (15 wt.% Co), at 550–650 °C under the same reaction conditions briefly mentioned above, and reported relatively low overall glycerol conversion values, with maxima of 52% at 550 °C [95]. Sanchez and Comelli used a Ni/Al (5.1 wt.% Ni) catalyst at 700 °C and at water/glycerol ratio of 3:1 (molar). They too did not analyze the liquid reaction products. They reported high H_2 production values, which they attributed to the high reaction temperature and related the deactivation of the catalysts to the formation of carbonaceous deposits [73]. Sanchez and Comelli [74] have also investigated the performance of Ni/Al (4 wt.% Ni), Co–Ni/Al (4 wt.% for each of Co and Ni) and a Co–Ni/Al (12 and 4 wt.% for Co and Ni respectively) catalysts at temperatures of 300, 500 and 700 °C at water/glycerol ratio of 6:1 (molar) and only reported on gaseous products. The authors concluded that the addition of Co promoted H_2 production, with the increase in Co loading improving performance only at low temperatures. Dou et al. [77] investigated the activity of a Ni–Cu/Al catalyst between 500 and 600 °C and at water/glycerol ratio of 9:1 (molar); they too only reported activity in terms of gaseous products. The authors reported moderate conversion values (also lower than those predicted thermodynamically) that ranged from 45% at 500 °C to 72% at 600 °C.

Table 1
Summary of the operating conditions used for the testing of different Ni, Co and Cu catalysts based on alumina for the GSR.

A/A	Active phase/Support	Reaction T (°C)	WGFR[a] (molar, unless otherwise stated)	GHSV[b] (unless otherwise stated)	Gas products (% mol/mol, dry basis, unless otherwise stated)	Liquid products	Ref
1	Ni (2%)/α-Al_2O_3	450–600	6:1	3.9×10^4 cm^3 h^{-1} g_{cat}^{-1}	$H_2 = 69.9$, $CH_4 = 1.6$, $CO = 8.9$, $CO_2 = 19.7$ (T = 600 °C)	1-Hydroxy-2-propanone, acetic acid, 1–2 propane diol, propanol, 2-methyl-2-cyclopentenone	[21]
2	Ni (4%)/Al_2O_3	300, 500, 700 (stability tests)	6:1	10 h^{-1} (WHSV[c])	$H_2 \approx 60$, $CH_4 \approx 1.4$, $CO \approx 14$, $CO_2 \approx 22$ (T = 700 °C, t < 5 h)	Not analyzed	[74]
3	Ni (5.1%)/Al_2O_3	700 (deactivation cycles)	3:1	5 h^{-1} (WHSV)	$H_2 \approx 78$, $CH_4 \approx 6$, $CO \approx 30$, CO_2 = n/a[d] (T = 700 °C, t < 5 h)	Not analyzed	[73]
4	Ni (10%)/Al_2O_3	600	9:1	3.09 g_{cat} h/$mol_{glycerol}$	$H_2 \approx 4$, $CH_4 \approx 0$, $CO \approx 0.5$, $CO_2 \approx 1.2$ (mol)	Not analyzed	[68]
5	Ni (10%)/Al_2O_3 (xerogel pretreated at 700, 800, 900, 1000 °C)	600	6:1	n/s[d]	$H_2 \approx 45$, CH_4 = n/a, CO = n/a, CO_2 = n/a (xerogel pretreated at 800 °C)	Not analyzed	[69]
6	Ni (13%)/Al_2O_3	500–600	10 wt.% glycerol	7.7 h^{-1} (WHSV)	$H_2 \approx 5$, CH_4 = n/a, CO = n/a, CO_2 = n/a (mol)	Acetaldehyde, acrolein, propanal, acetone, acetic acid, methanol, ethanol, 1,2-propylene glycol	[71,80]
7	Ni (Ni = 15%)/Al_2O_3 (calcined at 750, 850, 950 °C)	600, 800	36 wt.% glycerol	10,000 h^{-1}	$H_2 \approx 65$, $CH_4 = 5.5$, CO = n/a, CO_2 = n/a	Not analyzed	[88]
8	Ni (15%)/Al_2O_3	450–550	60–30 wt.%	5.0×10^4 mL g_{cat}^{-1} h^{-1}	$H_2 \approx 92$, $CH_4 = 18$, $CO = 22$, $CO_2 = 60$ (T = 550 °C)	Not analyzed	[22]
9	Ni (30% Ni)/Al_2O_3	550–800	3:1	5000–30,000 $mL_{C_3H_8O_3}$ h^{-1} mL_{cat}^{-1}	H_2, CH_4, CO, CO_2 (H_2 yield ≈1 mol of H_2/mol $C_3H_8O_3$ converted, T = 800 °C, t < 5 h)	Acetone, acetaldehyde, ethanol, propanol, acetic acid, 2,3-dyhydroxylpropanal	[59]
10	Co (15%)/Al_2O_3	550–650	60–30 wt.%	5.0×10^4 mL g_{cat}^{-1} h^{-1}	$H_2 \approx 25$, $CH_4 \approx 20$, $CO \approx 14$, $CO_2 \approx 10$ (T = 550 °C, t < 4 h)	Not analyzed	[95]
11	Co–Ni (5% Co, 10% Ni)/Al_2O_3	600–650	30–60 wt.% glycerol	5.0×10^4 mL g_{cat}^{-1} h^{-1}	Carbon deposition studies	Not analyzed	[91]
12	Co–Ni (4% Co, 4% Ni)/Al_2O_3	300, 500, 700	6:1	10 h^{-1} (WHSV)	$H_2 \approx 60$, $CH_4 \approx 8$, $CO \approx 8$, $CO_2 \approx 22$ (T = 700 °C, t < 5 h)	Not analyzed	[74]
13	Co–Ni (12% Co, 4% Ni)/Al_2O_3	300, 500, 700	6:1	10 h^{-1} (WHSV)	$H_2 \approx 50$, $CH_4 \approx 8$, $CO \approx 25$, $CO_2 \approx 15$ (T = 700 °C, t < 5 h)	Not analyzed	[74]
14	Ni–Cu (not specifying %)/Al_2O_3	500–600	9:1	n/s	$H_2 \approx 70$, CH_4 = n/a, CO = n/a, CO_2 = n/a (T = 800 °C)	Not analyzed	[77]
15	Ni–Cu (29%NiO, 31% CuO, 40% Al_2O_3)/Al_2O_3	450–650	n/s	n/s	$H_2 \approx 10$, $CH_4 = 0$, $CO = 1$, $CO_2 = 2$ (T = 650 °C)	Not analyzed	[24]

[a] WGFR = Water to Glycerol Feed Ratio.
[b] GHSV = Gas Hour Space Velocity.
[c] WHSV = Weight Hour Space Velocity.
[d] n/sa = not specified.

Based on this background, in the present study we report on the catalytic performance of nickel, cobalt and copper catalysts deposited on a commercial γ-Al_2O_3 support. The catalysts were synthesized via the incipient wetness impregnation method and had the same metal loading (8 wt.%). The synthesized samples, at their calcined and/or reduced form, were characterized by BET, ICP, XRD, DRS, NH_3-TPD, CO_2-TPD, TPR and SEM. The carbon deposited on their surface under reaction conditions was characterized by TEM, TPO, TGA and Raman. Catalytic performance for the glycerol steam reforming reaction was studied in order to investigate the effects of reaction temperature on: (i) glycerol total conversion, (ii) glycerol conversion to gaseous products, (iii) hydrogen selectivity and yield, (iv) selectivity to carbonaceous gaseous products, (v) selectivity to liquid products and (vi) molar ratios of H_2/CO and CO/CO_2 in the gaseous products' mixture. The stability of all catalytic samples was also investigated through time on stream experiments.

2. Materials and methods

2.1. Catalysts preparation

A commercial γ-Al_2O_3 (Akzo) was used as the supporting material of the nickel (Ni), cobalt (Co) and copper (Cu) based catalysts (SSA = 281 m^2 g^{-1} and Vp = 0.65 mL g^{-1}). As the support was in pellet form, it was first crashed and then sieved to 350–500 μm, before being calcined at 800 °C for 4 h. The samples were prepared using the incipient wetness impregnation technique (alternatively known as dry impregnation technique), by impregnating the γ-alumina with $Ni(NO_3)_2$ $6H_2O$, $CO(NO_3)_2$ $6H_2O$ and $Cu(NO_3)_2$ $6H_2O$, aqueous solutions (Sigma Aldrich) having the appropriate concentration (C = 0.17 M), in order to obtain a nominal loading of 8 wt.% Ni, Co or Cu in the final catalysts. Care was taken so as the total volume of the impregnation solutions was equal with the total pore volume of the alumina used. The impregnation solution was added drop wise to the support and was mixed with it. After addition of the solution was complete the support became slightly wet. The impregnated samples were dried overnight and then calcined at 800 °C for 5 h. All solutions for the catalysts preparation utilized distilled and deionised pure water generated by NANOpure Diamond UV unit (Barnstead International). The catalysts have been labelled herein as Ni/Al, Co/Al and Cu/Al.

2.2. Catalysts characterization

The Specific Surface Areas (SSA) of the catalysts was determinerd by N_2 adsorption–desorption isotherms at −196 °C, following the Brunauer-Emmett-Teller (BET) technique at relative pressures in the range of 0.05–0.30. The apparatus used was the Nova 2200e (Quantachrome). SSA was measured for calcined samples.

The total pore volume (Vp) calculation was based on nitrogen volume at the highest relative pressure, whereas the average pore size diameter was determined by the Barrett-Joyner-Halenda (BJH) method. Prior to each measurement the sample was degassed at 350 °C for 5 h under vacuum. Vp was measured for calcined samples.

The total metal loading (wt.%) of the final catalysts was determined by Inductively Coupled Plasma Atomic Emission Spectroscopy (ICP-AES) on a Perkin-Elmer Optima 4300DV apparatus. The methodology used has been described previously [96]. ICP measurements were performed for calcined samples.

X-ray diffraction (XRD) was used for the determination of the catalysts' crystalline structure. The equipment used was a ThermoAl diffractometer, operating at 40 kV and 30 mA, with Cu K_α radiation ($\lambda = 0.154178$ nm). Diffractograms were recorded in the $2\theta = 10$–$70°$ range at a scanning rate of 0.04° over 1.2 min^{-1}. The diffraction pattern was identified by comparison with those of known structure in the International Centre for Diffraction Data database. The XRD technique was used for both calcined and reduced samples.

The diffuse reflectance spectra (DRS) of the calcined samples were recorded in the range 200–800 nm at room temperature. The apparatus and procedure used has been described previously [101]. Briefly, a UV–Vis spectrophotometer (Varian Cary 3) equipped with an integration sphere has been used. Polytetrafluoroethylene (PTFE) was used as reference. The samples were mounted in a quartz cell. This provided a sample thickness >3 mm to guarantee the "infinite" sample thickness.

The surface acidity of the catalytic materials was investigated employing temperature programmed desorption of ammonia (NH_3-TPD) and carbon dioxide (CO_2-TPD) using the apparatus and following the procedure described in detail elsewhere [102]. In a typical experiment, a pre-weighed amount (100 mg) of the catalyst sample was placed in a quartz microreactor and reduced in situ with H_2 at 400 °C for 30 min. The sample was then cooled down to room temperature (RT) under flowing He and the flow was switched to a NH_3/He (or 10 v/v % CO_2/He) mixture for 60 min (or 30 min) for the NH_3-TPD (or CO_2-TPD) experiments. Finally, the system was purged with flowing He and the temperature was increased linearly from RT to 750 °C with a heating rate of 10 °C min^{-1}. Desorbed molecules were analyzed with the use of a mass spectrometer connected on line at the reactor effluent.

Temperature Programmed Reduction (H_2-TPR) experiments were performed by loading 100 mg of the catalyst in a U-type quartz tube adapted to a continuous flow TPR/TPD apparatus coupled with mass spectrometry, using the apparatus and following the procedures described in detail elsewhere [103]. Briefly, a total flow of 16 mL min^{-1} was employed as feed, with a H_2 content of 1 v/v % in He. Reactor temperature was programmed to start from ambient temperature and ramp up to 950 °C, at a rate of 10 °C min^{-1}. The influent and effluent gases were analyzed by MS. The main m/z fragment registered was $H_2 = 2$. Samples were pre-treated at 200 °C for 1 h under He flow and then cooled down to room temperature under the same atmosphere before the TPR spectra acquisition.

Transmission electron microscopy (TEM) micrographs of spend samples were obtained on a JEOL JEM-2100 system. Scanning electron microscopy (SEM) images of reduced catalysts were obtained using a JEOL 6300 microscope equipped with an energy dispersive spectrometer (EDS) for the determination of the chemical composition and element distribution of the samples [104].

The carbonaceous deposits on the spent catalysts were measured by Temperature Programmed Oxidation (TPO), as described elsewhere [104]. Briefly, the catalyst sample was heated linearly (10 °C min^{-1}) from RT to 750 °C under 20 v/v % O_2/He flow. The signals of O_2, CO and CO_2 were continuously monitored by an MS detector (FL-9496 Balzers). Calibration of MS signals was performed with the use of self-prepared gas mixtures of known concentration.

The amount of carbon deposited on the catalysts was additionally measured with a thermogravimetric analyzer (TGA), on a Leco TGA701 instrument. In the procedure, 50 mg of the used sample were subjected to a flow of dry air (3.5 L min^{-1}), from RT to 1000 °C, at a heating rate of 10 °C min^{-1}.

Raman spectroscopy was used to characterize the coke deposited on spent catalyst samples. The equipment and methodology employed have been described in a previous publication [105]. In short, Raman spectra (each sample of spent catalyst was approximately 50 mg) were collected using a WITEC alpha300R micro-Raman system (RAMAN Imaging System WITEC alpha300R). Spectra were acquired with a 20× long distance objective (0.35 numerical aperture) in the back-scattering geometry with an excitation wavelength of 532 nm from an Ar^+ ion laser (laser power set at 2 mW calibrated against a silicon standard). For each sample, at least three Raman spectra were collected in different areas to assess the homogeneity of the investigated material. All spectra collected from same samples showed similar features confirming the homogeneity of the carbon deposits.

2.3. Catalysts testing

The glycerol steam reforming (GSR) reaction was carried out at atmospheric pressure, in a continuous flow, fixed-bed, single pass, tubular stainless steel reactor, with an inner diameter of 14 mm, at temperature ranging from 400 to 750 °C. The experimental set up used allowed the feeding of both liquid and gaseous streams, having two vaporizers and a pre-heater before the reactor and a condenser after it. The vaporizers, pre-heater and reactor were placed into electrical ovens and regulated with programmed-temperature controllers.

Prior to catalytic testing, 200 mg of undiluted catalyst (the catalyst bed was supported by quartz wool) was reduced in situ under a flow of 100 v/v % hydrogen (100 mL min^{-1}) at 800 °C for 1 h. The catalyst was then purged with helium for 45 min, the temperature was lowered to 750 °C and the reaction feed was introduced into the catalyst bed. In order to ensure operation at steady state conditions, the catalyst was left for approximately 50 min at each step. Liquid products were obtained at the end of this 50 min period. The same procedure described above was also followed for the time on stream experiments. The difference was that temperature was reduced to 600 °C, catalytic stability was tested for 20 h, and measurements were taken every 1 h for the gaseous products and every 4 h for the liquid products.

The reaction feed consisted of the liquid stream - an aqueous solution of 20:80 wt.% $C_3H_8O_3$ and H_2O (20:1 steam/glycerol molar ratio), with a total liquid flow rate of 0.12 mL min^{-1}, which was kept under continuous stirring at room temperature - and the gas stream (Helium 5.0, 38 mL min^{-1}). The glycerol used had 99.5% purity and was obtained from Sigma Aldrich. The water/glycerol mixture was fed with a HPLC pump (Series I) into the evaporator and was first vaporized at 350 °C before it was mixed with helium. To prevent overpressure phenomena, pressure controllers were placed before and after the inlet and outlet gas, respectively. The gas feed at the reactor's inlet consisted of a gas mixture of 73% H_2O, 4% glycerol and 23% helium, corresponding to a Weight Hour Space Velocity (WHSV) of 50,000 mL g^{-1} h^{-1}. The reactor's outlet gases passed through a cold trap for liquid products capture.

The gaseous products were analyzed on-line by a gas chromatograph (Agilent 7890A), with two columns in parallel, HP-Plot-Q (19095-Q04, 30 m length, 0.530 mm I.D.) and HP-Molesieve (19095P-MSO, 30 m length, 0.530 mm I.D.), equipped with TCD and FID detectors. Liquid products were analyzed via a combined system of a Gas Chromatograph (Agilent 7890 A, with a 5MS column, equipped with an FID detector) and a Mass Spectrometer (Agilent 5975C). The schematic flow chart of the experimental setup is shown in Fig. 1S, along with detailed information regarding liquid product analysis.

2.4. Reaction metrics

Catalytic performance is reported in terms of H_2 yield, H_2, CO, CH_4 and CO_2 selectivity, glycerol conversion into gaseous products, and total glycerol conversion. Moreover, the performance of the catalysts for the liquid phase products is reported in terms of acetol ($C_3H_6O_2$), acetone [$(CH_3)_2CO$], allyl alcohol ($CH_2{=}CHCH_2OH$), acetaldehyde (C_2H_4O), acetic acid (C_2H_4O) and acrolein (C_3H_4O) selectivity. Performance parameters were calculated based on Eqs. (12)–(17):

$$\%\ \text{Glycerol conversion}_{(\text{global conversion})} = \left(\frac{\text{Glycerol}_{\text{in}} - \text{Glycerol}_{\text{out}}}{\text{Glycerol}_{\text{in}}}\right) \times 100 \tag{12}$$

$$\%\ \text{Glycerol conversion}_{(\text{gaseous products})} = \left(\frac{\text{C atoms in the gas products}}{\text{total C atoms in the feedstock}}\right) \times 100 \tag{13}$$

$$H_2\ \text{yield} = \frac{H_2\ \text{moles produced}}{\text{moles of glycerol in the feedstock}} \tag{14}$$

$$\%\ H_2\ \text{selectivity} = \left(\frac{H_2\ \text{moles produced}}{\text{C atoms produced in the gas phase}}\right) \times \frac{1}{RR} \times 100 \tag{15}$$

where, RR is the reforming ratio (7/3), defined as the ratio of moles of H_2 to CO_2 formed.

$$\%\ \text{selectivity of}\ i = \left(\frac{\text{C atoms in species}\ i}{\text{C atoms produced in the gas phase}}\right) \times 100 \tag{16}$$

where, species i refers to CO, CO_2, and CH_4.

$$\%\ \text{selectivity of}\ i' = \left(\frac{\text{C atoms in species}\ i'}{\text{C atoms produced in the liquid phase}}\right) \times 100 \tag{17}$$

where, species i' refers to acetol, acetone, allyl alcohol, acetaldehyde, acetic acid and acrolein.

The absence of significant external (intraparticle) mass and heat transfer limitations and internal (interparticle) mass transfer limitations for the GSR under the experimental conditions used herein was confirmed using the Mears and Weisz-Prater criterion values (relevant information are presented in the supplementary materials file).

3. Results and discussion

3.1. Catalyst characterization

3.1.1. Physicochemical properties of catalytic samples

The physicochemical properties of the calcined samples are listed in Table 2. It is observed that calcination at 800 °C resulted in a significant decrease of the specific surface area (SSA) of the Al_2O_3 support from 281 $m^2\ g^{-1}$ to 195 $m^2\ g^{-1}$, whereas the pore volume remained unaffected. Further reduction of the SSA occurred with the addition of Ni, Co or Cu on the supporting material; the pore volume was reduced marginally. The sample that suffered the greatest SSA reduction was the Cu/Al catalyst, i.e., from 195 $m^2\ g^{-1}$ to 142 $m^2\ g^{-1}$, whilst the reduction was slightly less marked for the Ni/Al (158 $m^2\ g^{-1}$) and Co/Al (154 $m^2\ g^{-1}$) catalysts. The catalysts' lower surface area can be attributed to the fact that the internal surface area of the support pore system is progressively covered by nickel, cobalt or copper species forming a layer [96,106,107]. Regarding the metal loading (wt.%), the ICP results indicate that the desired level was achieved in all samples.

Table 2
Characterization techniques results of the samples Al, Ni/Al, Co/Al, Cu/Al after calcination.

Catalyst/Support	SSA ($m^2\ g^{-1}$)	V_p (ml g^{-1})	Metal loading (wt.%)
Al	195	0.65	–
Ni/Al	158	0.57	7.88
Co/Al	154	0.58	7.42
Cu/Al	142	0.58	7.35

3.1.2. X-ray diffraction analysis

Fig. 1(a), (b), and (c) depicts the XRD patterns of the Ni/Al, Co/Al, and Cu/Al catalysts, respectively. In regards to the Ni/Al sample (Fig. 1a), γ-Al_2O_3 has been observed at 2θ = 37.2°, 47.2° and 67.6°. The absence of peaks corresponding to transition aluminas (2θ = 25.6° and 43.3° for θ-alumina, and 2θ = 31.2° and 36.6° for alpha-alumina) indicates that the calcination temperature used for this sample, i.e., 800 °C, was not high enough to bring about a transformation of the alumina. The formation of the spinel nickel aluminate phase ($NiAl_2O_4$), due to the reaction of NiO and Al_2O_3 at high calcination temperatures [108,109], was confirmed by peaks at 2θ = 19.0°, 32.0°, 37.0°, 45.0° and 60.2°. The absence of the nickel oxide (NiO) structure (expected at 2θ = 43.5° and 63.1°) can be either related to the size of these structures (i.e., they are smaller than 2–5 nm which is the typical XRD detection limit) [110] or to its nearly amorphous structure [94]. Two major differences can be observed between the calcined and reduced samples; the first, is the decreasing intensities of Al_2O_3 and $NiAl_2O_4$, and the second difference, is the appearance of small peaks due to the presence of metallic nickel (Ni^0) at 2θ = 44.0° and 51.2° (the low intensity of these peaks can be ascribed to the size of the metallic nickel species) [111,112]. Fig. 1(b) shows the XRD patterns of the Co/Al catalyst. The presence of the cobalt aluminate spinel phase ($CoAl_2O_4$) is verified by the appearance of diffraction lines at 2θ = 19.0°, 31.3°, 37.0°, 45.4°, and 59.5°. However, the cobalt oxide phase (Co_3O_4), was not detected, probably because its diffraction lines coincide with those of $CoAl_2O_4$; it is therefore difficult to distinguish between the two phases with this technique [113,114]. Llorca et al., suggested that at operating reforming reaction temperatures exceeding 400 °C, the Co_3O_4 phase transforms to cobalt oxide (CoO) and then to metallic cobalt (Co^0) [115,116]. The differences between the calcined and reduced Co/Al samples are similar to those of the Ni/Al catalyst; that is decreasing intensities of Al_2O_3 and $CoAl_2O_4$, and the appearance of two small peaks (at 2θ = 44.3° and 51.6°) due to the presence of metallic Co^0, in the reduced samples. Fig. 1(c) shows the XRD patterns of the calcined and reduced Cu/Al catalyst which are characterized by peaks corresponding to the copper aluminate spinel phase ($CuAl_2O_4$), located at 2θ = 19.0°, 32.0°, 36.7° and 60.2°. The peaks of γ-Al_2O_3 and $CuAl_2O_4$ decrease in intensity upon reduction. However, this is not accompanied by the detection of peaks attributable to metallic copper (Cu^0).

3.1.3. UV–Vis DRS analysis

Fig. 2 illustrates the diffuse reflectance (DR) spectra of the prepared catalysts recorded in the range 200–800 nm. An intense doublet with maxima at 595 and 630 nm appears in the spectrum of the Ni/Al catalyst. This doublet is assigned to Ni^{2+} ions in tetrahedral symmetry and is thus associated to the formation of the $NiAl_2O_4$ phase detected by XRD. Two shoulders appearing at 560 and 715 nm are assigned to Ni^{2+} ions in octahedral symmetry associated with the NiO phase [108]. For the Co/Al catalyst, three well-defined absorption bands are observed at 550, 580, and 625 nm ($^4A_2(F) \rightarrow {}^4T_1(P)$ transitions) indicating the presence of Co^{2+} ions in tetrahedral coordination. The weak shoulder peak observed at 480 nm ($^4T_{1g}(F) \rightarrow {}^4T_{1g}(P)$ transition) can be attributed to octahedral Co^{2+} ions [117]. Herein, it is suggested that the dispersed Co^{2+} ions mainly enter the tetrahedral vacancies of γ-Al_2O_3, which is supported by results of previous publications [118]. Regarding the Cu/Al catalyst, the environment in the neighborhood of Cu^{2+} ions can be identified by the charge-transfer bands shown in the spectrum. The main band with a maximum intensity around 260–330 nm can be attributed to the ligand-to-metal charge-transfer (LMCT) transition between Cu^{2+} and O^{2-} ions located on the catalyst's surface [119], whereas the less intense broad band ranging from 600 to

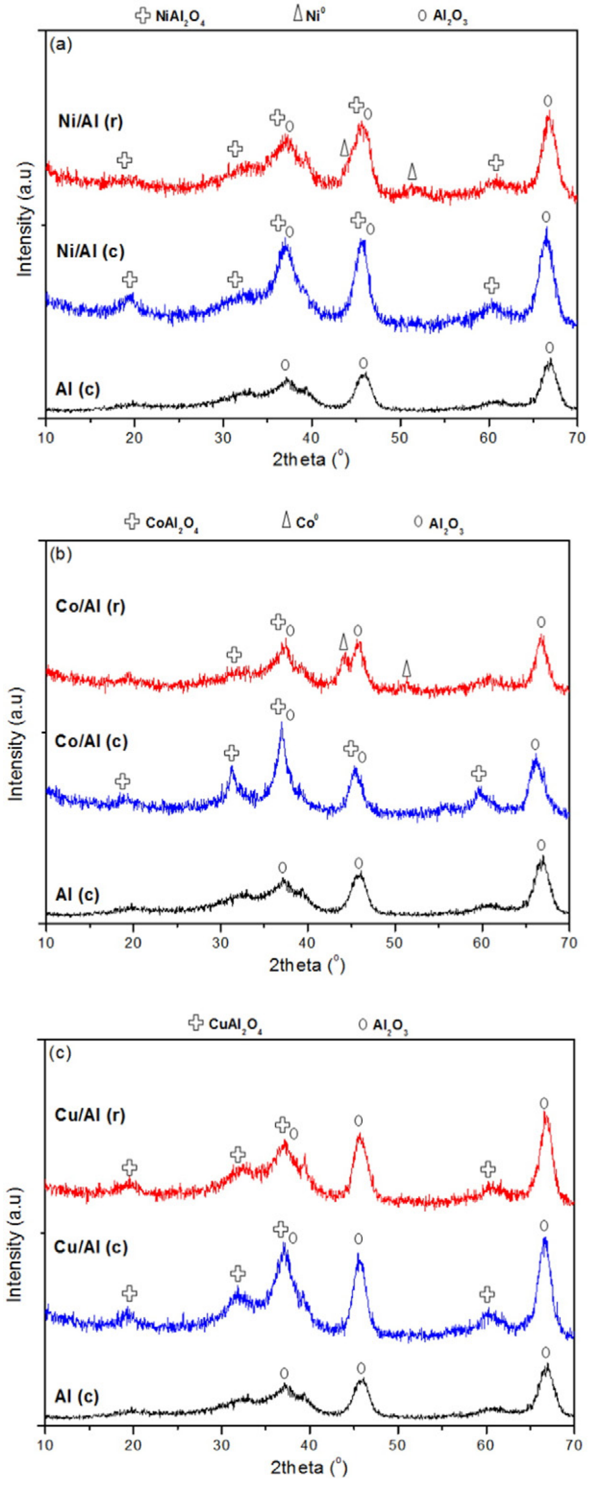

Fig. 1. XRD patterns of calcined and reduced catalysts inluding the calcined alumina support (a) Ni/Al, (b) Co/Al, and (c) Cu/Al.

800 nm indicates the presence of copper species in the octahedral coordination [120].

3.1.4. Surface acidity estimation

The NH_3-TPD patterns obtained for the studied catalysts are shown in Fig. 3(a), where the MS signal of desorbed ammonia is plotted as a function of temperature. The absence of other desorption products, such as H_2 or N_2, indicates that adsorption/desorption of NH_3 takes place molecularly over these materials. It is observed that all TPD curves are characterized by the presence of an intense desorption peak, located at ca. 85 °C, and a broad asymmetric decaying "tail" which extends to temperatures higher than 500 °C. The relative intensity of the low-temperature peak is considerably higher for the Cu/Al catalyst, compared to the other samples. Regarding the Ni/Al catalyst, desorption of ammonia is observed to continue at higher temperatures, with a relatively high amount desorbing at 350 °C. As shown in Fig. 3a (inset), the highest amount of NH_3 desorbs from the Cu/Al catalyst, indicating the presence of a higher number of acidic sites among the samples investigated. However, it is evident from the NH_3-TPD curves that the high acidity of the Cu/Al catalyst is mainly related to weaker sites, compared to the other samples.

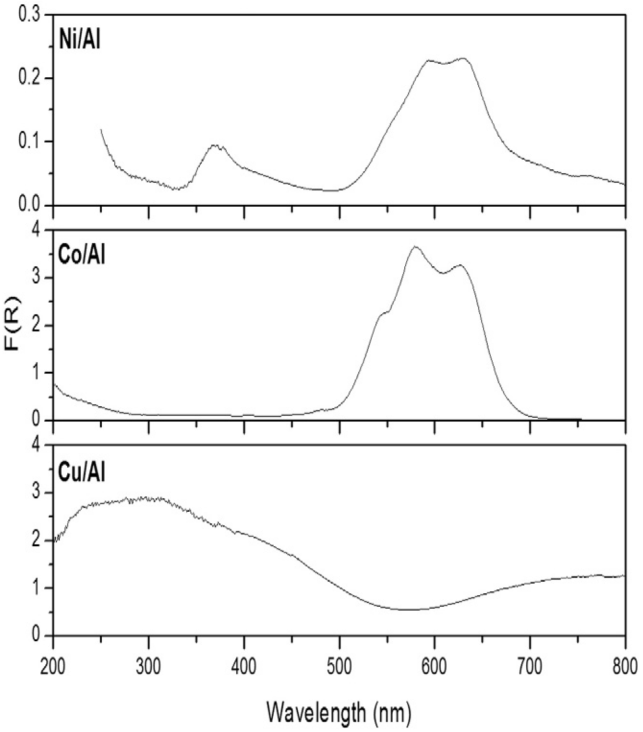

Fig. 2. UV–Vis DR spectra of calcined catalysts.

In Fig. 3(b) the CO_2-TPD profiles obtained for the four samples investigated are shown. It is observed that all desorption curves are characterized by the presence of a low temperature peak located at 65 ± 10 °C, which is significantly more intense for the Cu catalyst. The Ni-containing sample exhibits two additional high temperature peaks located at 225 °C and 495 °C, indicating the presence of stronger acidic sites on the catalyst surface. As shown in Fig. 3b (inset), the total amount of desorbed CO_2 is significantly higher for Cu/Al and Ni/Al catalysts, compared to Co/Al catalyst and bare Al_2O_3. These results show that the Cu/Al catalyst contains a higher amount of acidic sites, whereas the Ni/Al catalyst is characterized by the presence of stronger acidic sites, in agreement with results of the NH_3-TPD experiments (Fig. 3a).

3.1.5. Temperature programmed reduction

The oxidation state of the alumina-supported transition metals, as well as the catalysts' reducibility was investigated using Temperature Programmed Reduction (TPR). In order to characterize the type of reducible species present on the various catalysts, a Gaussian-type deconvolution was also applied (Fig. 4). From this fitting procedure several reduction peaks could be resolved for each catalyst. Regarding the Ni/Al sample, the small peak observed at low temperatures can be attributed to the reduction of bulk nickel oxide phase (α-peak), whereas the broad reduction band at T > 450 °C, which corresponds to the nickel aluminate structures (β-peak at 652 °C and γ-peak at 747 °C), indicate the existence of strong interaction between

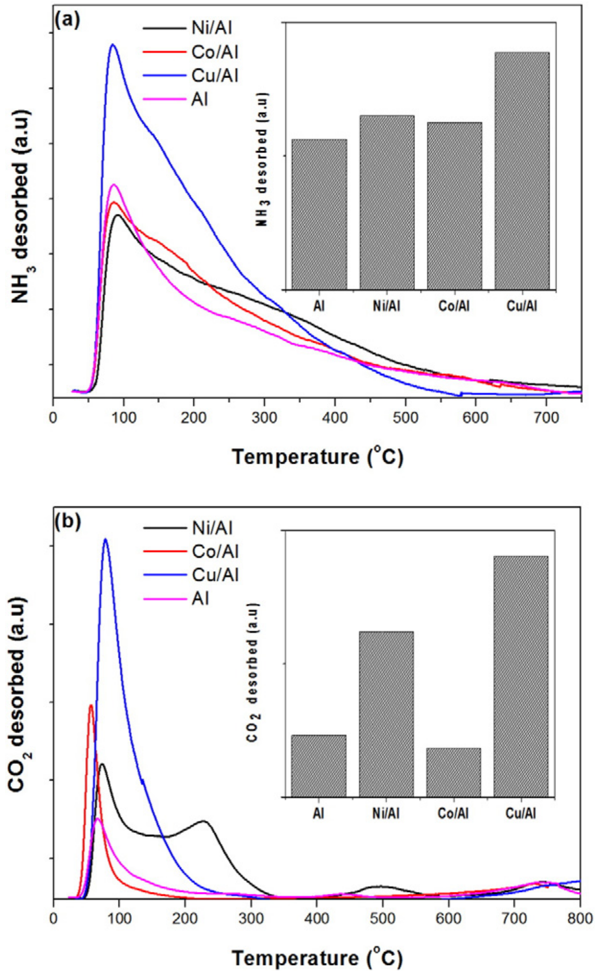

Fig. 3. (a) NH_3-TPD profiles and relative amount of NH_3 desorbed (inset), and (b) CO_2-TPD profiles and relative amount of CO_2 desorbed over (inset).

the dispersed nickel species and the alumina support. It can be also noticed that the characteristic reduction peak attributed to bulk NiO is almost negligible. The contribution of the β- and γ-peaks to the observed reduction peaks, as well as their position, can be related to the different Ni^{2+} coordination in the spinel framework. The estimated (from the deconvolution curves) contribution of the β-peak in the total Ni species present in the spinel structure of the Ni/Al catalyst was 53%, indicating that the surface nickel aluminate phase with a high degree of nickel-saturation was almost equal with the one with the low degree of nickel-saturation [121].

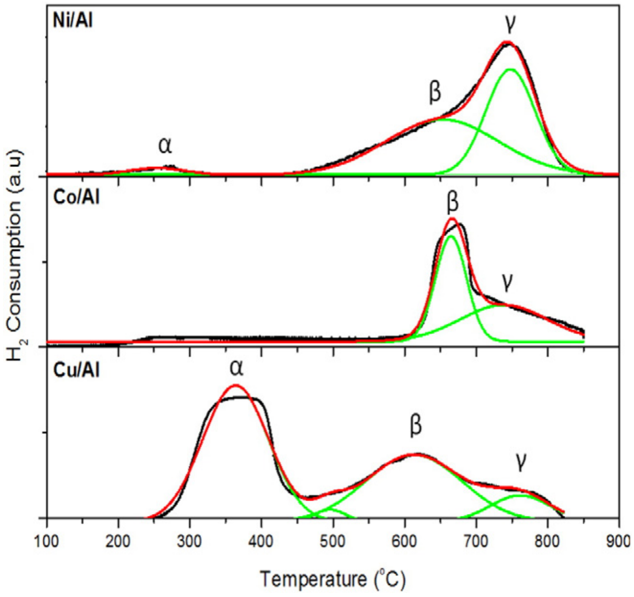

Fig. 4. TPR profiles of catalytic samples.

The TPR profile of the Co/Al catalyst exhibits two reduction peaks at high temperatures with their maxima located at 664 and 742 °C. The first peak can be attributed to the reduction of CoO particles to metallic cobalt and to cobalt species interacting strongly with the support, while the second peak could be attributed to the reduction of cobalt aluminates [122]. The cobalt aluminates are due to the strong interaction between Co_3O_4 and the support and can be formed by the introduction of Co(II) in the tetrahedral vacancies of the defect spinel structure of alumina. According to the literature [122,123] the dispersion of Co^{3+} and Co^{2+} ions on the catalyst surface and the migration of Co^{2+} ions into the lattice of Al_2O_3, occupying tetrahedral positions of the spinel, could be related to the higher temperature reduction peaks. This would depend on the amount of Al^{3+} ions present in the vicinity of cobalt ions, which in turn depends on the calcination temperature. In the present case, the estimated (from the deconvolution curves) contribution of the β-peak in the total Co species present in the spinel structure of the Co/Al catalyst was 51%. The absence of reduction peaks at low and medium temperatures can be attributed to the reduction of Co_3O_4 to CoO and of CoO to Co^0, respectively [123].

The Cu/Al catalyst is characterized by a broad reduction profile with peaks in both the low and high temperature zones. Dow et al. [124] have classified the reduction peaks on γ-alumina in terms of copper interaction with the surrounding atoms. The first reduction peak at 363 °C can be ascribed to first step reduction of accessible Cu^{2+} due to intra crystalline oxygen transfer from CuO. It can be also suggested that the sample has multiple reduction sites due to the presence of numerous small speaks of Cu-aluminate together with CuO. Thus, as the cell temperature rises, additional sites are activated resulting in secondary hydrogen consumption peaks by virtue of partial reduction of Cu-Al_2O_4 species to $CuAlO_2$. With further increase in temperature, the peak observed above 500 °C shows a second step reduction of Cu^{1+} which can be attributed to the reduction of isolated $CuAlO_2$ species to Cu^0 [125]. It is thus apparent that the considerable interaction of Cu with the support results in multiple reduction peaks and higher overall potential for reduction. As the γ-alumina has a defect spinel structure with Al^{3+} coordination in octahedral as well as tetrahedral position, which makes it highly active, copper loaded on γ-alumina has a higher tendency to form a spinel structure in the form of Cu-aluminate. It is known that the copper cation in "bulk" Cu-aluminate structure occupies both tetrahedral as well as octahedral position with the surrounding oxygen atoms [126,127]. Therefore, the estimated (from the deconvolution curves) contribution of the α-, β-, and γ-peak in the total copper species present in the Cu/Al catalyst was 51%, 39% and 9%.

3.1.6. Electron microscopy analysis

Fig. 5(a–d) shows the TEM micrographs obtained for the studied catalysts and the bare Al_2O_3 support after the catalytic stability tests. In all cases, it is observed that exposure to reaction conditions results in the deposition of large amounts of carbon, which covers practically the entire catalyst surface. As indicated in Fig. 5(c), two different types of carbon can be distinguished, namely filamentous carbon (whisker type) and graphene-like carbon. Filamentous carbon is well formed and has a narrow whisker diameter on the nickel catalyst (Fig. 5d) whereas all the other catalysts show signs of both wide and narrow whiskers. SEM images of the freshly reduced Ni/Al, Co/Al and Cu/Al catalysts can be found in Fig. 2S. EDS mapping shows that the latter elements are distributed homogeneously on the Al_2O_3 surface.

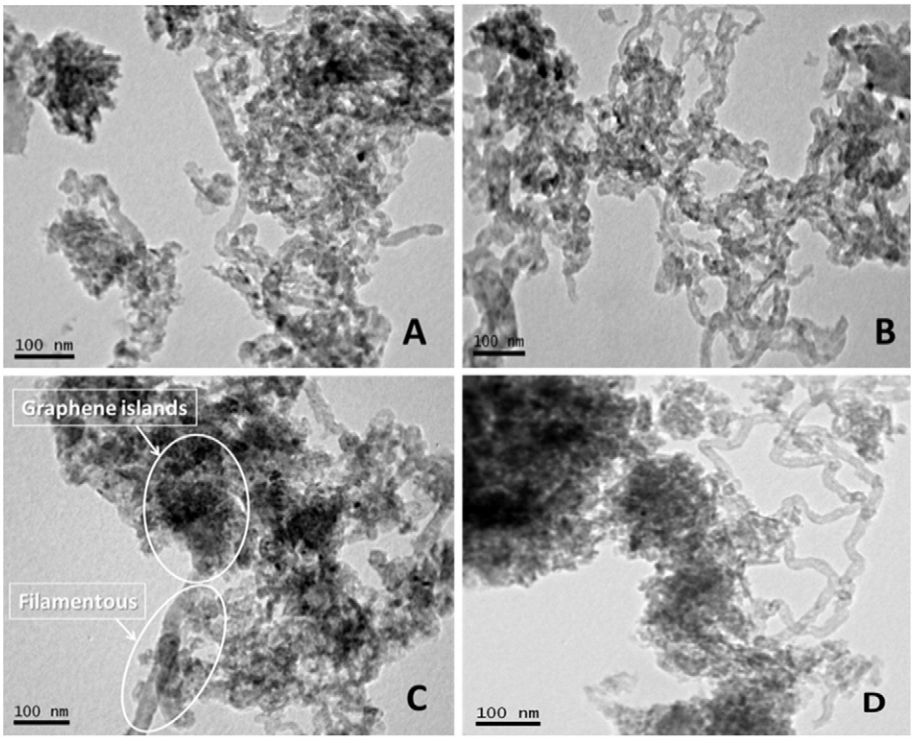

Fig. 5. TEM micrographs of used catalysts obtained after exposure to time on stream experiments (a) Alunina, (b) Co/Al, (c) Cu/Al, and (d) Ni/Al.

3.1.7. Temperature programmed oxidation

Results of TPO experiments obtained for the spent catalysts and the Al_2O_3 support after the stability tests are summarized in Fig. 6, where the CO_2 concentration at the reactor effluent is plotted as a function of temperature. It is observed that the TPO profile of Al_2O_3 is characterized by the presence of two features, a relatively intense doublet at 560/580 °C and a weaker peak at 645 °C. A qualitatively similar profile is observed for the Co/Al catalyst, although the peaks appear at lower temperatures (525/540 and 630 °C). The profile of the Ni/Al catalyst is characterized by the presence of only the double peak, which is shifted to lower temperatures (500/525 °C), compared to the Co/Al catalyst. Finally the TPO profile of the Cu/Al catalyst exhibits a completely different curve, compared to other samples and is characterized by an intense peak located at 470 °C and two much smaller peaks at 320 °C and 610/650 °C. The total amount of carbonaceous deposits formed on the studied samples following exposure to reaction conditions was estimated by integration of the respective TPO curves (inset of Fig. 6). It is observed that the highest amount of carbon is deposited on the bare Al_2O_3 support, followed by the Co/Al catalyst. These findings are corroborated by TGA results with the carbon deposited being measured at 22.5, 26.9, 23.1 and 35.7 wt.% for the Ni/Al, Co/Al, Cu/Al and Al samples, respectively.

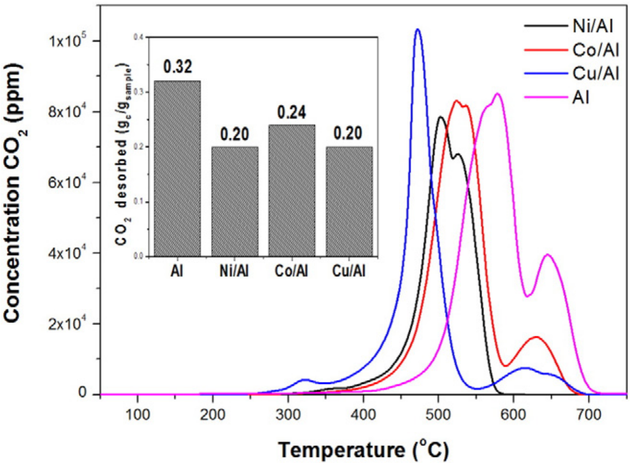

Fig. 6. TPO profiles and total amount of deposited carbon (inset) obtained for all samples after exposure to time on stream experiments.

3.1.8. Raman spectroscopy

The Raman spectra of all used catalytic samples after stability tests are shown in Fig. 7. In all cases, two characteristic peaks located at around 1344 and 1580 cm^{-1} can be observed. These peaks are attributed to the D-band (1344 cm^{-1}), associated with the disordered structural form of crystalline carbon species, and G-band (1580 cm^{-1}), corresponding to the graphitic carbon with high degree of crystallinity, order and symmetry [105]. The relative intensity of the D and G bands (I_D/I_G) gives valuable information about the degree of crystallinity of the carbon formed during the GSR reaction. Namely, smaller I_D/I_G value indicates higher crystallinity due to higher contribution of the graphitized carbon formed. Results of Fig. 7 show that the I_D/I_G ratio decreases in the following order: Ni/Al > Cu/Al > Co/Al > Al, indicating bare alumina exhibited the highest degree of carbon crystallinity ($I_D/I_G = 0.82$), while Ni/Al exhibited the highest degree of graphitization ($I_D/I_G = 1.53$) of the carbon species deposited. Raman spectroscopy of spent catalyst samples clearly confirms the formation of different carbon structures on the catalyst samples during GSR and indicates that the fraction of different carbon types formed depends on the type of active phase used.

3.2. Catalytic performance

3.2.1. Glycerol conversion

As mentioned above, the principal drawback of the GSR is its endothermicity, meaning that energy needs to be provided for the cleavage of the C—C, C—O and H—C bonds in the chain of the reactant. On the other hand, its main advantages in comparison to other

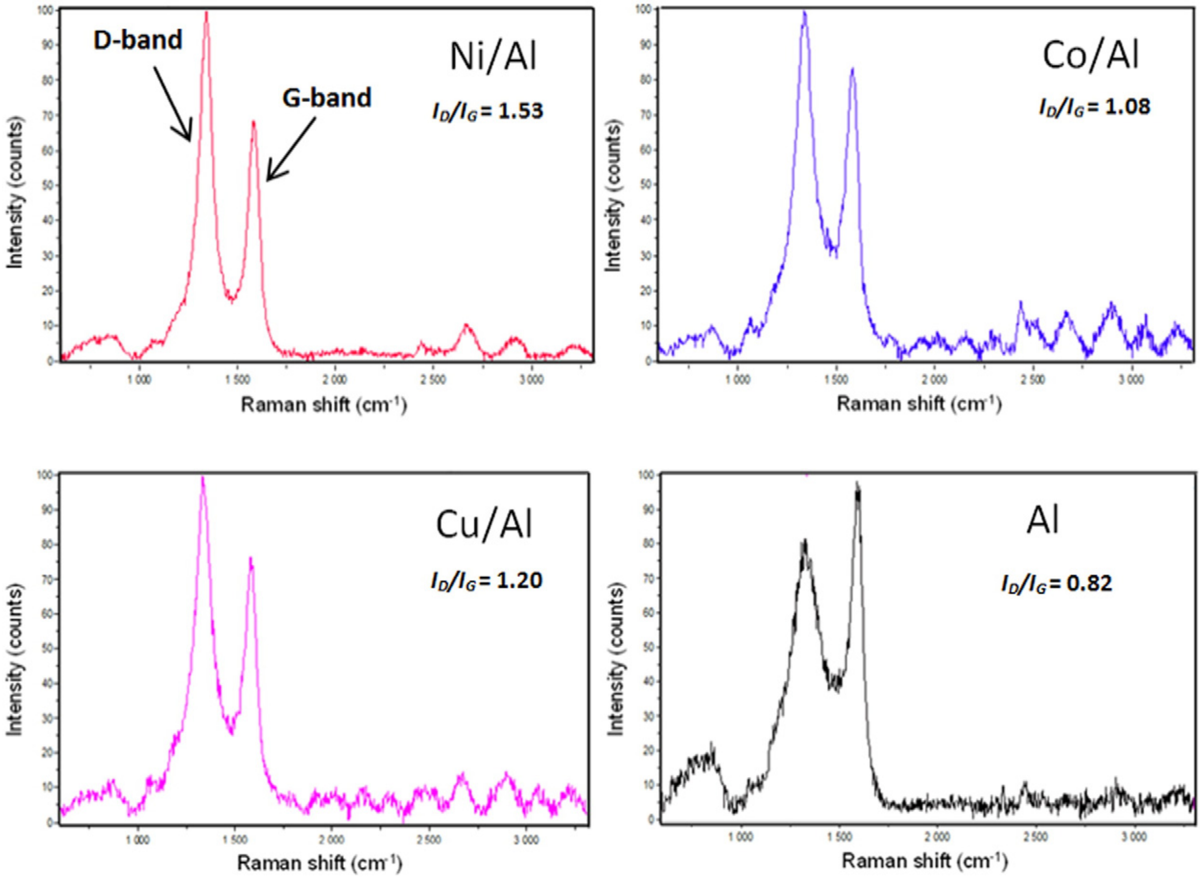

Fig. 7. Raman spectra of used samples after exposure to time on stream experiments.

reforming processes are that high concentration of hydrogen mixtures can be produced, accompanied by high conversion values of the reactants [128,129]. Previous studies of the GSR reaction have examined the performance of different catalytic systems at temperatures between 400 and 900 °C and GWFR of 3–12:1 (molar) [20–24,41–44,46,49–95]. In the present work the performance of the synthesized catalysts was investigated at temperatures in the range 400–750 °C and GWFR of 20:1 (molar).

Fig. 8 shows the dependence of the total glycerol conversion and the glycerol conversion to gaseous products on reaction temperature. As can be observed, both values increase with temperature (a consequence of the strongly endothermic nature of the GSR reaction). Specifically, glycerol's total conversion values range from 80% to 95% for the Ni/Al and Cu/Al catalysts, while the Co/Al catalyst seems to be less active (by about 5–10%), at least for the low reaction temperatures (400–550 °C). Above 600 °C, all samples exhibit similar conversion curves. As for the calcined alumina sample (Al), the same trend can be observed, with the only difference being that its conversion values are approximately 10% lower for the whole temperature range, in comparison to the metal loaded samples. The almost complete conversion of glycerol, which is suggested by the experimental results presented herein, is consistent with thermodynamic predictions [44–48,130,131].

As for the conversion of glycerol to gaseous products, it drastically increases with temperature; at 400 °C, X ≈ 7% for all samples whereas at 650 °C it takes values of ca. 86% for the Ni/Al and Cu/Al samples and ca. 77% for the Co/Al catalyst. A maximum conversion of gaseous products of ca. 92%) is achieved at 750 °C for all catalytic samples. In general, results presented in Fig. 8 show only small differences in the activity of Ni/Al, Co/Al and Cu/Al catalysts towards gaseous products, which is considerably higher than that of the calcined alumina (Al) sample.

The above mentioned findings are consistent with results of similar studies reported in the literature [33,60,66] which showed that the cleavage of the C—C or C—O bonds in the molecule of glycerol can be achieved only through a dehydrogenation step that can take place on the metal active sites. The higher contribution of the steam reforming reaction, compared with to glycerol decomposition when the temperature increases is also predicted by thermodynamics, as the steam reforming reaction is limited at low temperatures, where the water-gas shift and methanation reactions are favored.

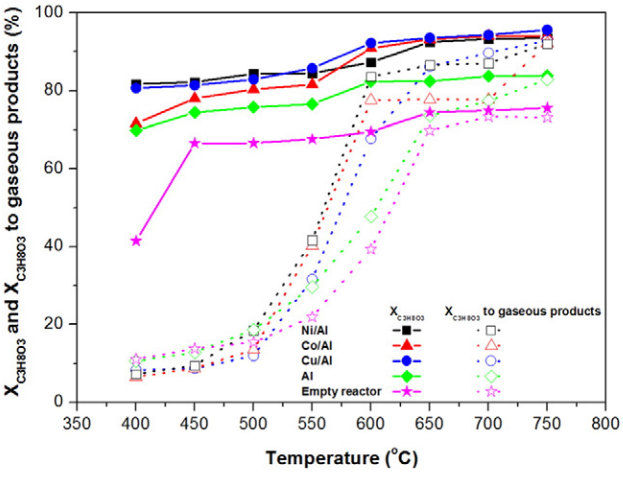

Fig. 8. Total glycerol conversion and glycerol conversion into gaseous products for all samples [Reaction conditions: $C_3H_8O_3$ (20 wt. %)/H_2O (total liquid flow rate = 0.12 mL/min)/He = 38 mL/min, $w_{catalyst}$ = 200 mg, T = 400–750 °C].

The slightly improved selectivity of the Ni/Al catalyst towards gaseous products can be mainly attributed to the stronger capacity of nickel in the cleavage of the C—C bond. According to the literature, Ni/Al catalysts show high glycerol conversion and hydrogen selectivity, before they gradually deactivate due to the formation of carbon over their surface [132]. Nevertheless, it has also been reported that catalysts calcined at high temperatures, as in the present case, could inhibit the formation of carbon without affecting the glycerol conversion and hydrogen selectivity [88].

Regarding the cobalt catalysts, these have shown good performance in ethanol reforming for hydrogen production and are proposed as appropriate catalytic systems. However these catalysts have shown significant deactivation through sintering and surface cobalt deactivation [133–135]. Even so, some authors have investigated the catalytic behavior of Co-based materials for GSR [62,95,136], while Co supported on alumina has been reported in a single work by Cheng et al. [95]. These researchers observed the existence of both strong and weak acid sites on the catalyst surface (with an acidic/basic ratio of about 6.0), while solid acidity increased with the addition of the Co species, as the calcination procedure probably enhanced weak acid site transformation to its strong acid counterpart [95].

As for Cu-based catalysts, it has also been proven that they are active for the ethanol steam reforming reaction, where it is believed that water promotes part of the copper species in an oxidized state and CO is rapidly oxidized to CO_2 before desorption [137–142]. In contrast to nickel, Cu is effective at breaking C—O bonds and avoids C—C bonds cleavages [143,144]. As a matter of fact, Sato et al. have used copper catalysts to produce 1,2-PDO with high yield, while they also observed that the addition of acidic oxide support such as Al_2O_3, ZrO_2, Fe_2O_3 and SiO_2 enhanced the selectivity to hydroxyacetone [145]. Despite our best efforts, we could not find any research works that reported on the performance of Cu based on alumina systems (in monometallic systems) for the GSR reaction.

Concluding, it can be stated that the Ni/Al catalyst reveals a slightly improved ability to convert glycerol into gaseous products, in comparison with the Co/Al and Cu/Al, most probably due to its superior capacity to promote the necessary C—C rupture. This is consistent with the literature, as it has been reported that Ni/Al_2O_3 catalysts with moderate Ni reduction degree, high Ni dispersion, and small nickel particle size could provide high H_2 yield for the glycerol steam reforming reaction. Studies have also shown that the GSR for hydrogen production occurs through glycerol dehydrogenation to leave CO bonded onto the catalyst surface, which could then undergo desorption, followed by the water gas shift or the methanation reaction [132]. As a matter of fact, by operating at high temperatures, it has been demonstrated that glycerol easily decomposes into CO, CO_2, olefins, water, hydrogen and oxygenates before reaching the catalytic surface. Therefore, catalytic considerations should take into account the ability of the active metal to activate C—O (typical of oxygenated compounds), C—C and C═C bonds [146–148].

3.2.2. Gaseous products selectivity

As mentioned above, thermodynamics suggest that the equilibrium composition of the gaseous products mixture depends on the steam to glycerol molar ratio in the feed, as well as the reaction temperature. In regards to the WGFR, the Le Chatelier principle is prevalent, meaning that H_2 production is favored when water is in excess. However, it has been reported that for very high WGFR (i.e. >12) the H_2 production increases at slow rates. Furthermore, by raising temperature hydrogen yield increases due to the boosting of the reverse methanation reaction (Eq. (5)). The production of CO, which is also favored at high temperatures, is usually attributed to the reverse water gas shift (RWGS) reaction. In contrast, at low temperatures, the production of CO_2 and CH_4 is prevalent because of the exothermic water gas shift and methanation reactions [44–48].

In the present work, GC analysis revealed that the main gaseous products were H_2, CO_2, CO and CH_4; ethylene (C_2H_4) was also detected but only in trace amounts. The influence of reaction temperature on hydrogen yield (Y_{H2}) and selectivity (S_{H2}) is shown in Fig. 9(a). As it can be observed, both values increase with increasing temperature following the thermodynamic analysis predictions. Specifically, S_{H2} ranges from 8 to 16% to 63%, 42% and 40% for the Ni/Al, Co/Al and Cu/Al catalysts, respectively. Concerning alumina, its capacity for hydrogen production was quite low, in comparison to catalytic samples, for the whole temperature range, especially for temperatures ranging between 450 and 650 °C. As for the Y_{H2} its maximum value was 4 mol for the Ni/Al, 3 mol for the Co/Al and Cu/Al and 2 mol per mole of glycerol for the Al sample at reaction temperatures ranging from 650 to 750 °C. This finding is in accordance with the thermodynamic analysis' predictions from Wang et al. [45] reporting that for WGFR equal to or higher than 9, the maximum theoretical value of hydrogen (6 mol) can be achieved at 652 °C. It can be also concluded that in the presence of the Ni/Al, Co/Al or Cu/Al catalyst the methane steam reforming reaction (Eq. (7)) is, in a different degree, accelerated with increasing temperature and variously contributes to the formation of hydrogen. Furthermore, the superior ability of the Ni/Al for H_2 production in comparison with the Co/Al and Cu/Al for the whole temperature range should be stated.

In Fig. 9 the influence of reaction temperature to the carbonaceous gaseous products' selectivity values, namely S_{CO_2}, S_{CO} (Fig. 9b) and S_{CH_4} (Fig. 9c) is presented. It can be observed that, for all catalysts, the reaction products' mixture was almost equimolar to the carbon oxides at low temperatures (400–450 °C), as their selectivity's values (S_{CO_2} and S_{CO}) were almost equal. By raising temperature, the CO selectivity increases reaching a maxima at 600 °C with the values of 79, 74 and 69% for the catalysts Ni/Al, Co/Al and Cu/Al, respectively. The opposite trend can be observed for the CO_2 selectivity; it decreases with increasing temperature for the low temperature range ($T < 600$ °C) and remains almost unaffected up to 750 °C to about 20% for all catalysts. As for the Al sample, a rather peculiar dependence can be observed, as S_{CO} starts from about 75% (400–450 °C) and then it reaches a minima to 60% at 500 °C, remaining rather stable with temperature for $T > 650$ °C. On the contrary, the S_{CO_2} values remain unaffected with increasing temperature for $T = 400–500$ °C; it drastically decreases from 30 to 10% for $T = 500–650$ °C and remains constant for $T = 650–750$ °C.

In Fig. 9(c) the influence of temperature on CH_4 selectivity is presented. As it can be observed for the Al sample, CH_4 selectivity is minimal for low reaction temperatures (400–550 °C), while it increases with increasing temperature (for $T > 550$ °C) reaching a plateau at 28% for temperature values higher than 650 °C. On the other hand, for all catalytic samples, methane selectivity decreases with increasing temperature; it takes its minimum value at 600 °C and reaches a plateau between 650 and 750 °C having values equal to 6, 10 and 18% for the Ni/Al, Co/Al and Cu/Al, respectively. The above findings are in good agreement with literature results, as it has been reported that for high water to glycerol feed ratios, as in our case, and at high temperatures (>650 °C), the formation of CH_4 should be inhibited, due to the methane steam reaction.

In Fig. 9(d) the influence of reaction temperature on the H_2/CO and the CO/CO_2 molar ratios in the gaseous products' mixture is shown. For the calcined alumina sample, it can be depicted that the H_2/CO molar ratio increases with increasing temperature, taking values ranging from 0.58 (400 °C) to 1.43 (750 °C). As for the CO/CO_2 molar ratio, it presents a rather peculiar trend, as it seems to be almost stable up to 450 °C, decreases for temperatures ranging between 450 and 500 °C, increases between 500 and 650 °C and has a descending trend for $T = 650–750$ °C; its maximum value equals to 5.34 for reaction temperature $T = 650$ °C. From Fig. 9(d) it can also be depicted that the H_2/CO molar ratio increases with increasing temperature for all catalysts, reaching a plateau at 500 °C and remaining unaffected up to 750 °C, taking the values of 2.03 for the Ni/Al sample and 1.5 for the Co/Al and Cu/Al catalysts. As for the CO/CO_2 molar ratio, the trend seems to be quite similar between the catalytic samples; it reaches a peak at 600 °C taking

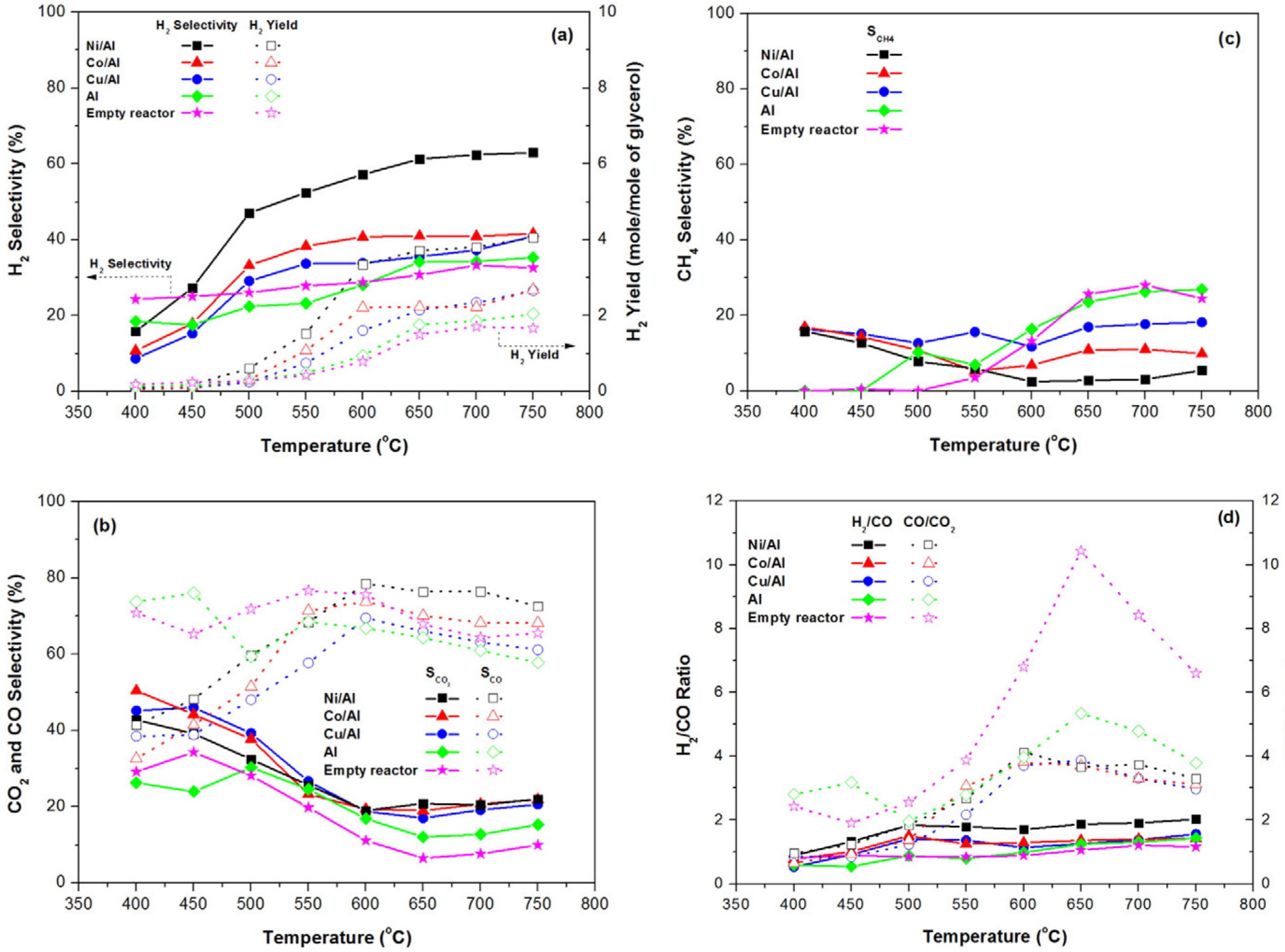

Fig. 9. (a) H_2 selectivity and H_2 yield, (b) CO_2 and CO selectivity, (c) CH_4 selectivity, and (d) H_2/CO and CO/CO_2 molar ratio [Reaction conditions: $C_3H_8O_3$ (20 wt.%)/H_2O (total liquid flow rate = 0.12 mL/min)/ He = 38 mL/min, $w_{catalyst}$ = 200 mg, T = 400–750 °C].

a value of 4.0 and descends to 3.0 (750 °C). This may indicate the presence of carbon deposits that may also react with the CO_2 formed according to the Boudouard reaction, thus altering the CO/CO_2 molar ratio as the reaction proceeds and the catalysts deactivate.

From the above findings, it has to be emphasized that for the case of the Ni/Al catalyst, the formation of CH_4 is almost inhibited for temperatures higher than 600 °C, which may be attributed to the methane steam reforming reaction. On the other hand, the production of CO at high temperatures for all catalysts can be attributed to the reverse water gas shift (RWGS) reaction. The ratio of CO/CO_2, increasing between 500 and 600 °C, points to the water gas shift reaction, caused by an increase in CO formation with increasing temperature [77].

Concluding, it has to be noticed that in accordance with the literature [95], in excess of steam, H_2, CO_2 and CO are the main gaseous products, with a lesser extent of CH_4 being produced. It should be also pointed out that the main difference between the Ni/Al and the Co/Al, Cu/Al catalysts was the larger H_2 amount and the lower CH_4 generation of the former, suggesting that the methane steam reforming reaction (Eq. (7)) is more pronounced for this case, especially at temperatures higher than 550 °C [149].

3.2.3. Liquid products selectivity

In Table 3 the liquid products' distribution for all samples (Ni/Al, Co/Al, Cu/Al, Al and empty reactor) at various reaction temperatures is shown. In agreement with previous works [23,80,146], the major products identified were acetaldehyde, acrolein, acetone, allyl alcohol, acetic acid and acetol, which were subsequently quantified. Other compounds were also identified, i.e., 2-Cyclopenten-1-one; 2-Cyclopenten-1-one, 2-methyl; Phenol; 2,3-Butanedione; Propylene glycol; 1,2-Ethanediol; Propanoic Acid; 2-Cyclohexen-1-one; 1,3-Dioxan-5-ol; and Phenol,2-methyl, but they were not quantified as they were in trace amounts.

The production of acetaldehyde, acetone, allyl alcohol, acetic acid and acetol can be observed for all of our experiments at temperatures lower than 650 °C; only acrolein was detected for T < 500 °C. An interesting observation is that some of the aforementioned compounds seem to be produced even at high temperatures for the Co/Al and Cu/Al catalysts (acetone at 750 °C, acetaldehyde, acetic acid and phenol at 700 °C). Compounds such as 2-cyclopenten-1-one and 2-cyclopenten-1-one, 2-methyl were detected for all samples at reaction temperatures between 500 and 600 °C. As for alumina, compounds such as acetone, acetic acid, acetol, phenol and 1,3-Dioxan-5-ol were produced for the whole temperature range. Moreover, 2,3-butanedione, propylene glycol and 1,2-ethanediol were identified as reaction products only for low reaction temperatures (T < 550 °C).

The liquid products' distribution observed confirms the complexity of the process, where the reactions of glycerol dehydration, dehydrogenation and hydrogenolysis are taking place [150,151]. Additionally, it could be evidenced that the produced intermediates can also be reformed, with the methane steam and dry reforming being considered as the main ones for temperatures above 700 °C, contributing to the carbon deposition on the catalysts' surface. Other reactions that can also be considered as thermodynamically feasible under reforming conditions are the deposited carbon steam gasification and hydrogenation, as well as the Boudouard reaction.

Table 3
Liquid products' distribution for all samples (Ni/Al, Co/Al, Cu/Al, Al) and the empty reactor at various reaction temperatures.

		Reaction temperature (°C)							
A/A	Compounds	400	450	500	550	600	650	700	750
1	Acetaldehyde	1,2,3,4,5	1,2,3,4,5	1,2,3,4,5	1,2,3,4,5	1,2,3,4,5	1,2,3,4,5	2,3,5	5
2	Acrolein	1,2,3,4,5	1,2,3,4,5	1,2,3,4,5					
3	Acetone	1,2,3,4,5	1,2,3,4,5	1,2,3,4,5	1,2,3,4,5	1,2,3,4,5	1,2,3,4,5	1,2,3,4,5	2,3,4,5
4	Allyl Alcohol	1,2,3,4,5	1,2,3,4,5	1,2,3,4,5	1,2,3,4,5	1,2,3,5	1,2,3,5	5	5
5	Acetic Acid	1,2,3,4,5	1,2,3,4,5	1,2,3,4,5	1,2,3,4,5	1,2,3,4,5	1,2,3,4,5	1,2,3,4,5	4,5
6	Acetol	1,2,3,4,5	1,2,3,4,5	1,2,3,4,5	1,2,3,4,5	1,2,3,4,5	1,2,3,4,5	4,5	4,5
7	2-Cyclopenten-1-one		2,4	1,2,3,4	1,2,3,4	2,3,4			
8	2-Cyclopenten-1-one, 2-methyl			1,3,4	1,2,3,4	3,4			
9	Phenol	1,4	1,4	1,2,4	1,2,3,4	1,2,3,4	2,3,4,5	2,3,4,5	4,5
10	Glycerol	1,2,3,4,5	1,2,3,4,5	1,2,3,4,5	1,2,3,4,5	1,2,3,4,5	1,2,3,4,5	1,2,3,4,5	1,2,3,4,5
11	2,3-Butanedione	2,3,4,5	1,2,3,4,5	1,2,3,4,5	1,3,4,5				
12	Propylene glycol	1,2,3,4,5	1,2,3,4,5	2,3,4,5	5	5			
13	1,2-Ethanediol	1,2,3,4,5	1,2,3,4,5	2,3,4,5	5	5	5	5	5
14	Propanoic Acid		1	1	3	3,4	2,3,4		
15	2-Cyclohexen-1-one	3							
16	1,3-Dioxan-5-ol	2,3,4,5	2,3,4,5	3,4,5	3,4,5	4,5	4,5	4,5	4,5
17	Phenol,2-methyl			3	3	3,4			

Note: 1 = Ni/Al, 2 = Co/Al, 3 = Cu/Al, 4 = Al, 5 = Empty reactor.

In Table 4 the concentration values (v/v %) of the main liquid products for the Ni/Al, Co/Al, Cu/Al, Al samples and empty reactor, at various reaction temperatures (400–750 °C), are presented. Acrolein is produced via glycerol dehydration [152–155] on acid sites. Allyl alcohol is formed from glycerol via hydride or hydrogen transfer mechanism. On the other hand, acetaldehyde can be formed from glycerol or acrolein [154,156]. A schematic representation of the different reaction pathways in the GSR is provided in Fig. 10.

In order to clarify the distribution of the reaction's main condensated products, the dependence of their selectivity values, namely acetol (S_{acetol}), acetone ($S_{acetone}$), allyl alcohol ($S_{allyl\ alcohol}$), acetaldehyde ($S_{acetaldehyde}$) acetic acid ($S_{acetic\ acid}$) and acrolein ($S_{acrolein}$) of the temperature, for all samples is shown in Fig. 11. Condensable products as acetol, acetaldehyde, acrolein have also found that were produced during the GSR by Araque et al. [64] and they have been considered as the main carbon precursors [152,157].

For the Ni/Al catalyst (Fig. 11a) it can be depicted that acetol, acetaldehyde, acetone, acetic acid and allyl alcohol were the main liquid products for T < 650 °C with their selectivity values ranging between 28 and 39%, 15–22%, 16–29%, 7–18% and 17–27%, respectively. For reaction temperature 700 °C, acetone (72%) and acetic acid (28%) were the only detectable compounds, while at 750 °C all glycerol in the feed has been converted to gaseous products. Indicatively, the values of liquid products' selectivities at 650 °C were: $S_{acetol} = 6\%$, $S_{acetone} = 29\%$, $S_{allylalcohol} = 27\%$, $S_{acetaldehyde} = 21\%$ and $S_{acetic\ acid} = 18\%$.

For the Co/Al catalyst, it can be observed (Fig. 11b) that acetol appeared to be the main liquid product for T < 600 °C, with its selectivity having values from 24 to 43%, while allyl alcohol decreases with temperature (up to T = 600 °C) from 34 to 13.5%. On the other hand, the selectivities of acetone, acetaldehyde and acetic acid increase with temperature (up to T = 650 °C); acetone was the only product detected at T = 750 °C. For this catalyst, the liquid products' selectivity values at 650 °C were as follows: $S_{acetol} = 1.2\%$, $S_{acetone} = 30\%$, $S_{allylalcohol} = 26\%$, $S_{acetaldehyde} = 21\%$ and $S_{acetic\ acid} = 22\%$.

For the Cu/Al catalyst (Fig. 11c), acetol was the main product for reaction temperatures lower than 600 °C, with selectivity values ranging from 11 to 38%. Other products as acetone, allyl alcohol, acetaldehyde and acetic acid selectivities and for the same temperature range, seems to be rather constant at values of 18%, 17%, 15% and 12%, respectively. Acetone (60.5%), acetaldehyde (20%) and acetic acid (20%) were detected at 700 °C, whereas acetone was the only liquid product at temperature as high as 750 °C. Indicative selectivity values at 650 °C were the following: $S_{acetol} = 11\%$, $S_{acetone} = 28\%$, $S_{allylalcohol} = 8\%$, $S_{acetaldehyde} = 26\%$ and $S_{acetic\ acid} = 27\%$.

As for the calcined alumina (Al) sample, from Fig. 11(d) it can observed that almost all of the main liquid products were detected even at T = 750 °C; with the exception of allyl alcohol and acetaldehyde that were not produced at temperatures higher than 600 and 700 °C, respectively. A decrease in the S_{acetol} and $S_{allyl\ alcohol}$ and an increase in the

Table 4
Concentration values (v/v %) of liquid products for the Ni/Al, Co/Al, Cu/Al, Al samples and the empty reactor at various reaction temperatures (400–750 °C) as determined by GC/MS analysis.

	Reaction temperature (°C)							
Product	400	450	500	550	600	650	700	750
Ni/Al								
Acetol	6.29	5.83	5.75	4.40	4.09	0.33	0.00	0.00
Acetone	4.28	3.82	3.21	2.66	1.81	1.67	1.23	0.00
Allyl alcohol	3.74	3.50	3.49	3.14	2.05	1.45	0.00	0.00
Acetaldehyde	6.21	5.07	3.64	3.11	2.02	1.39	0.00	0.00
Acetic acid	2.09	1.75	1.71	1.50	1.37	1.22	0.56	0.00
Acrolein	1.85	1.11	0.86	0.00	0.00	0.00	0.00	0.00
Co/Al								
Acetol	5.69	5.06	5.00	4.58	4.24	0.06	0.00	0.00
Acetone	3.42	2.64	2.54	2.20	2.06	1.63	1.29	1.13
Allyl alcohol	8.11	5.00	1.75	1.43	1.33	1.29	0.00	0.00
Acetaldehyde	3.92	2.90	1.82	1.57	1.35	1.31	0.91	0.00
Acetic acid	2.23	1.94	1.94	1.63	1.46	1.37	1.15	0.00
Acrolein	1.79	1.37	1.03	0.00	0.00	0.00	0.00	0.00
Cu/Al								
Acetol	5.89	5.67	5.16	3.92	2.53	0.45	0.00	0.00
Acetone	3.33	2.70	2.26	2.20	1.59	1.23	1.16	0.34
Allyl alcohol	4.27	2.28	1.89	1.72	1.40	0.33	0.00	0.00
Acetaldehyde	5.26	2.15	2.09	1.66	1.48	1.29	0.43	0.00
Acetic acid	2.08	2.07	1.65	1.65	1.43	1.38	0.45	0.00
Acrolein	4.16	2.58	2.11	0.00	0.00	0.00	0.00	0.00
Alumina								
Acetol	8.09	7.95	7.15	5.39	1.43	1.38	1.35	1.31
Acetone	5.95	5.87	4.85	4.43	3.50	3.11	2.48	1.00
Allyl alcohol	4.11	3.72	3.63	2.80	0.00	0.00	0.00	0.00
Acetaldehyde	6.57	5.97	5.56	5.49	3.19	2.51	0.00	0.00
Acetic acid	3.28	3.28	3.04	2.80	2.79	2.55	2.37	2.21
Acrolein	4.38	3.96	2.63	0.00	0.00	0.00	0.00	0.00
Empty reactor								
Acetol	8.82	8.55	7.49	7.42	7.35	4.07	1.42	1.22
Acetone	3.54	3.07	2.74	2.56	2.53	2.52	2.48	2.20
Allyl alcohol	6.27	5.60	4.45	4.06	3.72	2.93	2.23	1.00
Acetaldehyde	5.85	4.77	4.59	4.47	4.23	3.84	2.71	2.16
Acetic acid	3.77	3.64	3.20	3.12	2.97	2.92	2.82	2.40
Acrolein	3.11	2.47	1.22	0.00	0.00	0.00	0.00	0.00

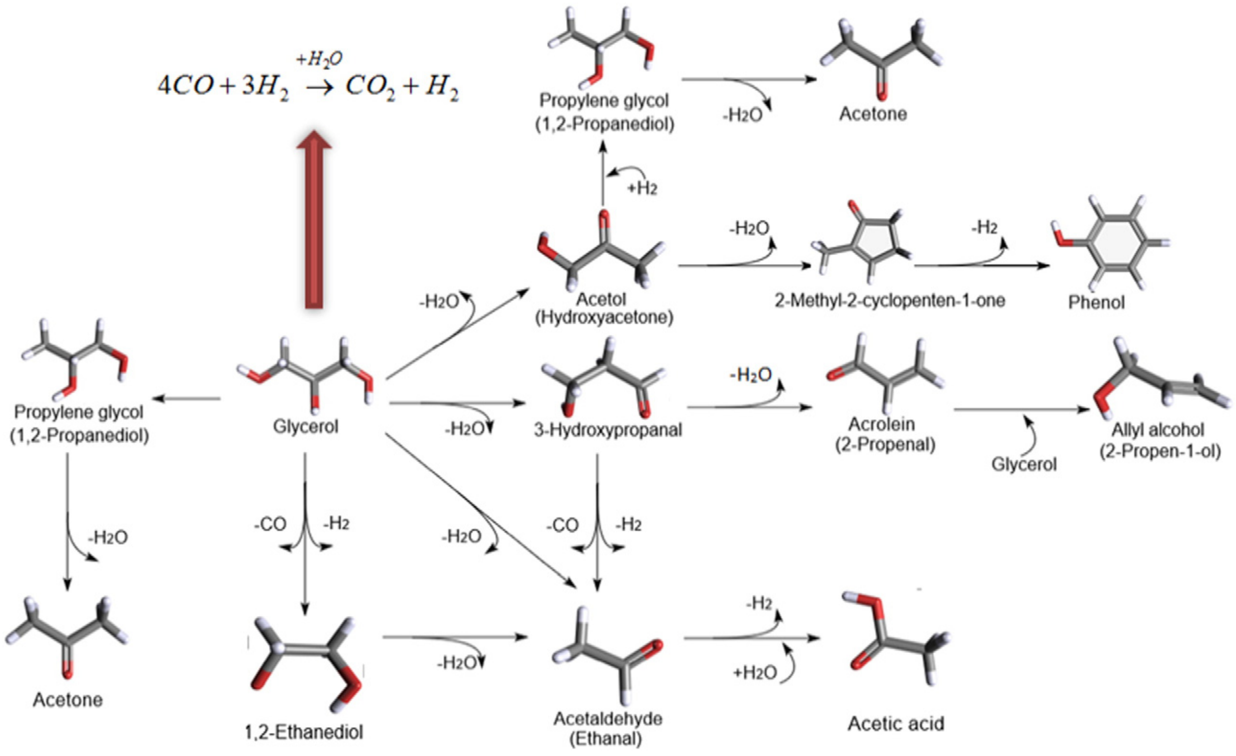

Fig. 10. Reaction pathway for the glycerol steam reforming reaction.

$S_{acetone}$, $S_{acetaldehyde}$ and $S_{acetic\ acid}$ can be also observed for temperatures lower than 650 °C. Some indicative selectivity values for 650 °C were as follows $S_{acetol} = 16.5\%$, $S_{acetone} = 35\%$, $S_{allylalcohol} = 0\%$, $S_{acetaldehyde} = 24\%$ and $S_{acetic\ acid} = 24\%$. For the homogeneous reaction (empty reactor) all of the main liquid products were detected even at temperatures as high as 750 °C.

A more detailed approach to the explanation of liquid products' distribution can be obtained by the reaction scheme shown in Fig. 10, where the conversion of glycerol to hydrogen takes place through the formation of a variety of chemical intermediates, such as alcohols and ketones. It can be suggested that since glycerol is not a thermally stable molecule the extent of pyrolysis phenomena plays an important role in the steam reforming conditions and likely the intermediates formed in the glycerol cracking are reformed in the catalysts surface. Having acid sites (mainly of Lewis type) alumina is not chemically inert, presenting catalytic properties for acid-base catalyzed reactions such as dehydration, isomerization and polymerization, that can also take place during glycerol steam reforming. In accordance with Bobadilla et al. [42] the presence of strong acid centers decreases the C—C bond breaking capacity favoring the coke deposition. Hydrogen is produced via the dehydrogenation of the adsorbed glycerol molecules and reaction of adsorbed organic fragments with hydroxyl groups, which migrate from the support to active phase crystallites/alumina interfaces. At low temperatures the formation of condensable products are favored, that being activated at higher ones they form intermediates leading to carbon oxides and hydrogen.

Concerning the acid-base properties, it is accepted that besides the quantity and strength of the acid sites, a balanced distribution of basic strength is also desirable; otherwise the selectivity and stability may be strongly affected [158]. Hernandez et al. [159] suggested that active sites for the glycerol conversion are not necessarily based on Ni^0, but it is the basicity of the catalysts (oxygen anion sites) which is the key parameter to form acetol and even break C—C bonds to a certain extent. Auroux et al., [160] have also observed that basic sites are important for acetol formation. Nevertheless, it has been demonstrated that the use of basic materials does not solely assure the stability of the catalyst for glycerol's steam reforming reaction [52]. Regarding acetaldehyde, it may be produced via partial decomposition of 3-hydroxypropanal [161] or through acetol formation [51,162]; the later appears a more probable path from the experimental results presented herein.

3.2.4. Catalyst's stability and carbon deposition

It is well known that catalyst deactivation in reforming reactions is mainly caused by carbon deposited on their surface. Thus, a great number of research works have been devoted in investigating its nature and its removal kinetics [78,163–167]. It has been suggested that atomic carbon or C_yH_{1-y} species (C_α species) is produced by dissociative chemisorption of the hydrocarbon on the catalytic surface. An amorphous film (C_β) may be produced by dehydropolymerization, which by further aging could lead to graphitic carbon. These carbon atoms, in some cases, could be also dissolved and diffused through the metal to active growth areas, in a way that amorphous vermicular (or whisker) carbon (C_γ) could be precipitated. Nickel and cobalt can be considered as metals that can dissolve the carbon atoms to form carbides, though this diffusion/precipitation step. Furthermore, the amorphous carbon can be converted into graphitic (C_δ), under severe and prolonged reaction conditions.

In Fig. 12 the stability results for the twenty (20) hours time on stream experiments for all catalysts are presented. A drastic drop in the activity of the Ni/Al catalyst can be observed for the first seven (7) hours, as values for glycerol total conversion and its conversion into gaseous products (Fig. 12a) decrease from 90% to 50% and from 80% to 10%, respectively. On the contrary, the Co/Al and Cu/Al catalysts seem to deactivate at a rather slower rate, as their values for glycerol total conversion and its conversion into gaseous products drop from 90% to 70% and from about 60% to 20%, respectively. From Fig. 12(b) it can be observed the dependence of H_2 yield and selectivity with time on stream. As can be seen, values of H_2 yield decrease with time for all catalysts, following a sharp decline curve for the Ni/Al (from 3.4 to 0.8) for the first five (5) hours. The decline was smoother for the Co/Al and Cu/Al catalyst starting from the value of 2.0 and reaching the value of 1.0 after 20 h. The opposite trend can be seen for the H_2 selectivity as it seems to be

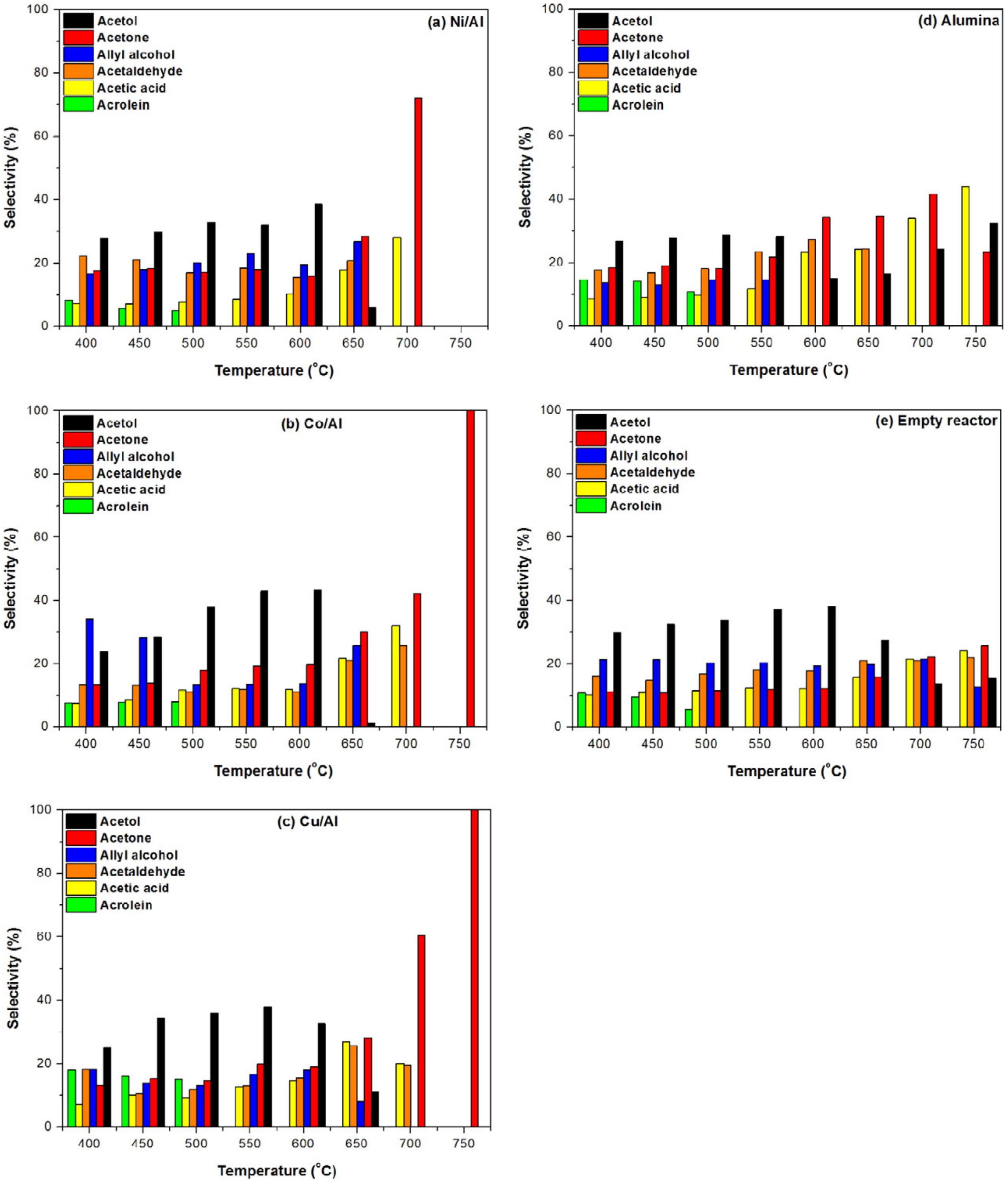

Fig. 11. Liquid products selectivity for: (a) Ni/Al, (b) Co/Al, (c) Cu/Al, (d) Alumina sample, and (e) Empty reactor [Reaction conditions: $C_3H_8O_3$ (20 wt. %)/H_2O (total liquid flow rate = 0.12 mL/min)/ He = 38 mL/min, $w_{catalyst}$ = 200 mg, T = 400–750 °C].

increasing with time for all catalysts. From Fig. 12(c) it can be seen that the CO and CO_2 selectivity values were quite constant after about 1 h in the reaction stream for the Co/Al and Cu/Al catalysts being equal to 80% and 20%, respectively. On the contrary, for the Ni/Al catalyst the S_{CO_2} and S_{CO} reveal a rather strange variation through reaction time as after a decline (rise) for the first two (2) hours these gradually increase (decrease) taking the values of 45% and 55%, respectively. As for the liquid products their concentration (selectivity) values seem to be quite constant for the whole reaction time.

In Table 5 the catalytic performance of the Ni/Al, Co/Al and Cu/Al samples described by the reaction metrics at 600 °C, at the beginning (1st measurement) and the end (after 20 h) of the time on stream experiments is shown. It should be stated that the study of carbon deposition on the catalytic surface during the GSR reaction is considered to be a major challenge by all researchers, e.g., [86,91,136]. As has been mentioned above, reactions that are though as responsible for coke accumulation are glycerol's thermal decomposition [131] and dehydration, as well as the dehydrogenation, and the condensation of its by-products

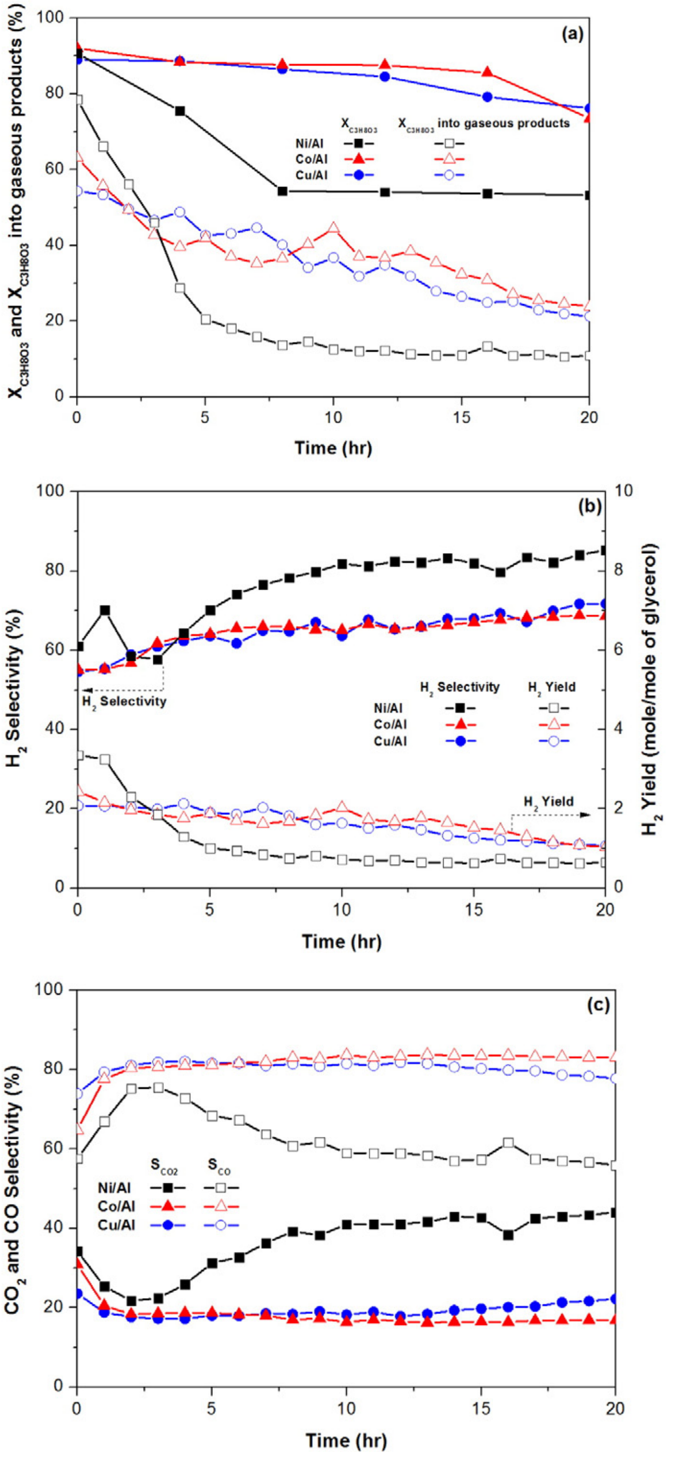

Fig. 12. Time on stream experiments (a) Total glycerol conversion and glycerol conversion into gaseous products, (b) H_2 selectivity and H_2 yield, and (c) CO_2 and CO selectivity [Reaction conditions: $C_3H_8O_3$ (20 wt. %)/H_2O (total liquid flow rate = 0.12 mL/min)/He = 38 mL/min, $w_{catalyst}$ = 200 mg, T = 600 °C, t = 20 h].

[168]. According to previously reported experimental and theoretical studies, a suppression of the coke formation could be accomplished with high values in reaction temperatures and steam to carbon (S/C) molar ratios, as well as, by adding oxygen in the feed [20,169–173].

Table 5
Catalytic performance of the Ni/Al, Co/Al and Cu/Al samples at 600 °C (first and last measurement of time on stream experiments.

Reaction metric	Ni/Al	Co/Al	Cu/Al
$X_{(C_3H_8O_3)}$, %	90.70 → 53.30	92.05 → 73.50	89.05 → 76.15
$X_{(C_3H_8O_3)\ \text{into gaseous products}}$, %	78.48 → 10.94	63.14 → 23.85	54.38 → 21.23
$Y_{(H_2)}$, %	3.35 → 0.65	2.43 → 1.04	2.08 → 1.07
$S_{(H_2)}$, %	61.04 → 85.31	55.05 → 68.66	54.58 → 71.75
$S_{(CO_2)}$, %	34.25 → 44.10	30.88 → 16.90	23.54 → 22.21
$S_{(CO)}$, %	57.54 → 55.90	64.80 → 83.10	73.92 → 77.79
$S_{(CH_4)}$, %	8.21 → 0.00	4.32 → 0.00	2.53 → 0.00
$S_{(\text{Acetol})}$, %	33.98 → 39.03	30.26 → 29.65	36.62 → 33.85
$S_{(\text{Acetone})}$, %	14.57 → 13.46	21.95 → 23.46	21.39 → 20.37
$S_{(\text{Allyl alcohol})}$, %	18.90 → 16.98	21.23 → 20.42	16.27 → 18.57
$S_{(\text{Acetaldehyde})}$, %	17.59 → 15.89	12.91 → 13.94	14.71 → 15.62
$S_{(\text{Acetic acid})}$, %	14.97 → 14.63	13.65 → 12.52	11.01 → 11.59
H_2/CO	2.48 → 3.56	1.98 → 1.96	1.72 → 2.15
CO/CO_2	1.68 → 1.27	2.10 → 5.10	3.14 → 3.50

From Table 5, it is clear that the Ni/Al catalyst had the highest values in terms of glycerol conversion to gaseous products values (78.5%), H_2 yield (3.4), H_2 (61.0%), CO_2 (34.2%), CH_4 (8.1%), acetaldehyde (17.6%) and acetic acide (15.0)selectivity, and H_2/CO molar ratio (2.5) values, at the beginning of the reaction. Moreover, it exhibits the lowest selectivity values for CO (57.5%), acetone (14.6%) and CO/CO_2 molar ratio (1.7) values, among all samples. It can be observed that these values change with time on stream, making it the worst catalyst, after a drastic deactivation occurred during the first 7 h. For nickel based on alumina, Raman results showed the presence of graphitic carbonaceous deposits on its surface [73,79,92,174]., In accordance with NH_3-TPD and CO_2-TPD results, it has been proposed [97] that coke deposition, associated with the dehydration, cracking and polymerization reactions, takes place on the catalyst's surface strong acid sites. As reported by Pant et al. [79], besides carbon deposition, sintering could be another reason for the Ni/Al_2O_3 catalysts deactivation. It has also been suggested that the transition of alumina's crystalline phase during the reaction could be associated with the Ni active phase's sintering [98].

Regarding the Co/Al catalyst, it exhibited the highest values at the end of the time on stream experiments for conversion to gaseous products (23.8%), CO (83.1%), acetone (23.5%) and allyl alcohol (20.4%) selectivity, as well as CO/CO_2 molar ratio (5.1) and the lowest for H_2 (68.7%), CO_2 (16.9%), acetol (29.6%) and acetaldehyde (13.9%). Generally, for cobalt-based catalysts, the mechanisms that have been reported in the literature, attribute deactivation to three main reasons: (i) the oxidation and sintering of the metallic phase, (ii) the transformation of the solid state that involves the diffusion of cobalt into the support forming irreducible cobalt support compounds (e.g. aluminates and silicates), and (iii) the formation of inert carbon phases (also confirmed by TPO and Raman results presented herein) that block the cobalt active sites [175,176]. Moreover, a relationship between the catalytic performance of catalyst and the molar ratio of Co^{2+}/Co^0 was established for the ethanol steam reforming reaction; deactivation of catalysts mainly occurred by carbon deposition. However, the control of Co^{2+}/Co^0 ratio helped to equilibrate the steps of ethanol activation and carbon oxidation, resulting in stable catalysts [177].

As for the Cu/Al sample, it can be seen that it exhibits the highest value for total glycerol conversion (76.1%) and H_2 yield (1.07), but the lowest values for acetic acid selectivity (11.6%) at the end of the time on stream experiments. On the other side at the beginning of the reaction, it exhibits the lowest values for glycerol's conversion to gaseous products (54.4%), for H_2 production (Y_{H_2} = 2.1, S_{H_2} = 54.6%), for CO_2 (23.5%), allyl alcohol (16.3%) and acetic acid selectivity, as well as for H_2/CO (1.72) molar ratio, among all catalysts. In addition, it reveals the highest values for CO (73.9%) and acetol (36.6%) selectivity and CO/CO_2 molar ratio (3.14) between all samples. It is noted that the Cu/Al catalyst had the higher amount of weaker acid sites (Fig. 3) a medium ratio of I_D/I_G (Fig. 7), while the total amount of carbonaceous deposits (Fig. 6) was comparable with the other two samples. This finding is in accordance with the literature [143] as it is well known that glycerol's dehydration route becomes more pronounced when Cu is the active phase for the steam reforming reaction. The dehydration route markedly contributes to the carbon deposition on the catalysts as noted by previous works leading to the observed deactivation [178]. The formation of carbon deposits during dehydration reaction of glycerol may result from consecutive reactions of glycerol, like oligomerization on acidic catalyst surface sites and/or side reactions between dehydrated products like hydroxyacetone [156].

It should be emphasized the crucial role of the catalyst's specific characteristics on the reaction product's distribution, as the pathways resulting in coke formation, such as thermolysis, oligomerization, olefin formation, via e.g. dehydration and decarbonylation should be carefully tailored, having in mind that carbon gasification reaction may be rather kinetically slow. Strategies that have been used for the active phase's sintering alleviation, aim to strengthen the interactions between the catalytically active site and the support's surface (strong metal-support interaction, SMSI) by using other supporting materials as CeO_2 [86], TiO_2, or ZrO_2 [72] or by incorporating promoters like alkaline ions [179].

4. Conclusions

In this contribution a study of supported on γ-alumina transition metals', catalytic performance for the GSR reaction is reported. Catalysts with active phase nickel (Ni), cobalt (Co) or copper (Cu) were synthesized, via the incipient wetness impregnation method at a series of constant loading (8 wt.%). From the NH_3-TPD and CO_2-TPD results it can be suggested that the Cu catalyst contains a higher amount of acidic sites, whereas the Ni catalyst is characterized by the presence of stronger acidic sites. The presence of nickel and cobalt aluminate structures in the calcined Ni/Al and Co/Al samples was confirmed by XRD, DRS and TPR with an almost equal contribution of the β- and γ-peak. As for the Cu/Al sample, it has multiple reduction sites due to the presence of numerous small speaks of Cu-aluminate together with CuO, as it was found to have a broad reduction profile with peaks in both low and high temperature zones.

Two different types of carbon can be distinguished, namely filamentous carbon (whisker type) and graphene-like carbon from the TEM micrographs obtained for the spent samples after time on stream experiments. The total amount of carbon was measured by TPO and TGA and followed the order Ni/Al < Co/Al < Cu/Al. Raman spectroscopy of spent catalysts clearly confirms the formation of different carbon structures on the catalyst samples during GSR and indicates that the fraction of different carbon types depends on the type of active phase used.

The Ni/Al catalyst reveals an improved ability to convert glycerol into gaseous products, in comparison with the Co/Al and Cu/Al, most probably due to its superior capacity to promote the necessary C—C rupture. It also has a superior ability for H_2 production while the formation of CH_4 is almost inhibited for temperatures higher than 600 °C, which may be attributed to the methane steam reforming reaction. The production of CO at high temperatures for all catalysts can be attributed to the reverse water gas shift (RWGS) reaction.

As for the liquid products, the production of acetaldehyde, acetone, allyl alcohol, acetic acid, acrolein and acetol can be observed for all experiments at temperatures lower than 650 °C, while their distribution confirms the complexity of the process, where reactions of glycerol dehydration, dehydrogenation and hydrogenolysis are taking place. Specifically, for the Ni/Al catalyst, acetol, acetaldehyde, acetone acetic acid and allyl alcohol were the main liquid products, while for the Co/Al and Cu/Al catalysts the main product appeared to be. Regarding acetaldehyde, it may be produced via partial decomposition of 3-hydroxypropanal or through acetol formation; the later appears a more probable path from the experimental results presented herein. A drastic drop in the activity of the Ni/Al catalyst can be observed for the first seven (7) hours, while the Co/Al and Cu/Al catalysts seem to deactivate at a rather slower rate. This confirms that coke deposition is associated with the dehydration, cracking and polymerization reactions that take place on the catalyst's surface strong acid sites.

Acknowledgements

Financial support by the program THALIS implemented within the framework of Education and Lifelong Learning Operational Program, co-financed by the Hellenic Ministry of Education, Lifelong Learning and Religious Affairs and the European Social Fund, Project: ‘Production of Energy Carriers from Biomass by Products. Glycerol Reforming for the Production of Hydrogen, Hydrocarbons and Superior Alcohols' is gratefully acknowledged (MIS: 379333). We are also grateful to Prof. Kordulis Christos (University of Patras), Prof. Yentekakis Ioannis (Technical University of Crete) and Assoc. Prof. Iordanidis Andreas (TEI of Western Macedonia) for kindly allowing us to make use of the facilities in their respective laboratories and perform the DRS, TPR and TGA experiments.

Appendix A. Supplementary data

Supplementary data to this article can be found online at http://dx.doi.org/10.1016/j.fuproc.2016.06.024.

References

[1] M. Hook, X. Tang, Depletion of fossil fuels and anthropogenic climate change-a review, Energy Policy 52 (2013) 797–809, http://dx.doi.org/10.1016/j.enpol.2012.10.046.

[2] A.P. Mathews, Renewable energy technologies: panacea for world energy security and climate change, Proc. Comp. Sci. 32 (2014) 731–737, http://dx.doi.org/10.1016/j.procs.2014.05.483.

[3] S. Pfenninger, J. Keirstead, Renewables, nuclear, or fossil fuels? Scenarios for Great Britain's power system considering costs, emissions and energy security, Appl. Energy 152 (2015) 83–93, http://dx.doi.org/10.1016/j.apenergy.2015.04.102.

[4] N. Abas, A. Kalair, N. Khan, Review of fossil fuels and future energy technologies, Futures 69 (2015) 31–49, http://dx.doi.org/10.1016/j.futures.2015.03.003.

[5] N.D. Charisiou, M.A. Goula, Attitudes of Greek university students towards energy and the environment, Glob. Nestle J. 16 (2014) 856–865.

[6] A.K. Azad, M.G. Rasul, M.M.K. Khan, S.C. Sharma, M.A. Hazrat, Prospect of biofuels as an alternative transport fuel in Australia, Renew. Sust. Energ. Rev. 43 (2015) 331–351, http://dx.doi.org/10.1016/j.rser.2014.11.047.

[7] Y. Su, P. Zhang, Y. Su, An overview of biofuels policies and industrialization in the major biofuel producing countries, Renew. Sust. Energ. Rev. 50 (2015) 991–1003, http://dx.doi.org/10.1016/j.rser.2015.04.032.

[8] L.E. Rincón, J.J. Jaramillo, C.A. Cardona, Comparison of feedstocks and technologies for biodiesel production: an environmental and techno-economic evaluation, Renew. Sust. Energ. Rev. 69 (2014) 479–487, http://dx.doi.org/10.1016/j.renene.2014.03.058.

[9] M. Guo, W. Song, J. Buhain, Bioenergy and biofuels: history, status, and perspective, Renew. Sust. Energ. Rev. 42 (2015) 712–725, http://dx.doi.org/10.1016/j.rser.2014.10.013.

[10] G. Nicoletti, N. Arcuri, G. Nicoletti, R. Bruno, A technical and environmental comparison between hydrogen and some fossil fuels, Energy Convers. Manag. 89 (2015) 205–213, http://dx.doi.org/10.1016/j.enconman.2014.09.057.

[11] US Energy Information Administration (EIA), International Energy Statistics, http://www.eia.gov/cfapps/ipdbproject/IEDIndex3.cfm 2015 (accessed at 30/5/2015).

[12] F. Murphy, G. Devlin, R. Deverell, K. McDonnell, Potential to increase indigenous biodiesel production to help meet 2020 targets - an EU perspective with a focus on Ireland, Renew. Sust. Energ. Rev. 35 (2014) 154–170, http://dx.doi.org/10.1016/j.rser.2014.03.046.

[13] T.M. Yunus Khan, A.E. Atabani, I.A. Badruddina, A. Badarudina, M.S. Khayoon, S. Triwahyono, Recent scenario and technologies to utilize non-edible oils for biodiesel production, Renew. Sust. Energy Rev. 37 (2014) 840–851, http://dx.doi.org/10.1016/j.rser.2014.05.064.

[14] I.M. Atadashi, M.K. Aroua, A.R. Abdul Aziz, N.M.N. Sulaiman, The effects of catalysts in biodiesel production: a review, J. Ind. Eng. Chem. 19 (2013) 14–26, http://dx.doi.org/10.1016/j.jiec.2012.07.009.

[15] W.N.M. Wan Ghazali, R. Mamat, H.H. Masjuki, G. Najafi, Effects of biodiesel from different feedstocks on engine performance and emissions: a review, Renew. Sust. Energ. Rev. 51 (2015) 585–602, http://dx.doi.org/10.1016/j.rser.2015.06.031.

[16] I. Contreras-Andrade, E. Avella-Moreno, J.F. Sierra-Cantor, C.A. Guerrero-Fajardo, J.R. Sodré, Purification of glycerol from biodiesel production by sequential extraction monitored by ^1H NMR, Fuel Process. Technol. 132 (2015) 99–104, http://dx.doi.org/10.1016/j.fuproc.2014.12.016.

[17] H. Rastegari, H.S. Ghaziaskar, From glycerol as the by-product of biodiesel production to value-added monoacetin by continuous and selective esterification in acetic acid, J. Ind. Eng. Chem. 21 (2015) 856–861, http://dx.doi.org/10.1016/j.jiec.2014.04.023.

[18] M. Pudukudy, Z. Yaakob, M. Mohammad, B. Narayanan, K. Sopian, Renewable hydrogen economy in Asia - opportunities and challenges: an overview, Renew. Sust. Energy Rev. 30 (2015) 743–757, http://dx.doi.org/10.1016/j.rser.2013.11.015.

[19] J.M. Silva, M.A. Soria, L.M. Madeira, Challenges and strategies for optimization of glycerol steam reforming process, Renew. Sust. Energy Rev. 42 (2015) 1187–1213, http://dx.doi.org/10.1016/j.rser.2014.10.084.

[20] S. Adhikari, S. Fernando, A. Haryanto, Production of hydrogen by steam reforming of glycerin over alumina-supported metal catalysts, Catal. Today 129 (2007) 355–364, http://dx.doi.org/10.1016/j.cattod.2006.09.038.

[21] I.N. Buffoni, F. Pompeo, G.F. Santori, N.N. Nichio, Nickel catalysts applied in steam reforming of glycerol for hydrogen production, Catal. Commun. 10 (2009) 1656–1660, http://dx.doi.org/10.1016/j.catcom.2009.05.003.

[22] C.K. Cheng, S.Y. Foo, A.A. Adesina, Steam reforming of glycerol over Ni/Al_2O_3 catalyst, Catal. Today 178 (2011) 25–33, http://dx.doi.org/10.1016/j.cattod.2011.07.011.

[23] A. Iriondo, V.L. Barrio, J.F. Cambra, P.L. Arias, M.B. Güemez, R.M. Navarro, M.C. Sanchez-Sanchez, J.L.G. Fierro, Influence of La_2O_3 modified support and Ni and Pt active phases on glycerol steam reforming to produce hydrogen, Catal. Commun. 10 (2009) 1275–1278, http://dx.doi.org/10.1016/j.catcom.2009.02.004.

[24] A. Wang, B. Dou, C. Chen, Y. Song, Y. Xu, X. Du, L. Zhang, T. Luo, C. Tan, Renewable hydrogen production from steam reforming of glycerol by Ni–Cu–Al, Ni–Cu–Mg, Ni–Mg catalysts, Int. J. Hydrog. Energy 38 (2013) 3562–3571, http://dx.doi.org/10.1016/j.ijhydene.2013.01.042.

[25] F.D. Alvarado, F. Gracia, Oxidative steam reforming of glycerol for hydrogen production: thermodynamic analysis including different carbon deposits representation and CO_2 adsorption, Int. J. Hydrog. Energy 37 (2012) 14820–14830, http://dx.doi.org/10.1016/j.ijhydene.2012.01.158.

[26] K. Kamonsuangkasem, S. Therdthianwong, A. Therdthianwong, Hydrogen production from yellow glycerol via catalytic oxidative steam reforming, Fuel Process. Technol. 106 (2013) 695–703, http://dx.doi.org/10.1016/j.fuproc.2012.10.003.

[27] G. Yang, H. Yu, F. Peng, H. Wang, J. Yang, D. Xie, Thermodynamic analysis of hydrogen generation via oxidative steam reforming of glycerol, Renew. Energy 36 (2011) 2120–2127, http://dx.doi.org/10.1016/j.renene.2011.01.022.

[28] G. Yang, H. Yu, X. Huang, F. Peng, H. Wang, Effect of calcium dopant on catalysis of Ir/La_2O_3 for hydrogen production by oxidative steam reforming of glycerol, Appl. Catal. B Environ. 127 (2012) 89–98, http://dx.doi.org/10.1016/j.apcatb.2012.08.003.

[29] P.J. Dauenhauer, J.R. Salge, L.D. Schmidt, Renewable hydrogen by autothermal steam reforming of volatile carbohydrates, J. Catal. 244 (2006) 238–247, http://dx.doi.org/10.1016/j.jcat.2006.09.011.

[30] H. Wang, X. Wang, M. Li, S. Li, S. Wang, X. Ma, Thermodynamic analysis of hydrogen production from glycerol autothermal reforming, Int. J. Hydrog. Energy 34 (2009) 5683–5690, http://dx.doi.org/10.1016/j.ijhydene.2009.05.118.

[31] Y. Liu, A. Lawal, Kinetic study of autothermal reforming of glycerol in a dual layer monolith catalyst, Chem. Eng. Process. 95 (2015) 276–283, http://dx.doi.org/10.1016/j.cep.2012.06.012.

[32] N. Hajjaji, I. Baccar, M.N. Pons, Energy and exergy analysis as tools for optimization of hydrogen production by glycerol autothermal reforming, Renew. Energy 71 (2014) 368–380, http://dx.doi.org/10.1016/j.renene.2014.05.056.

[33] R.D. Cortright, R.R. Davda, J.A. Dumesic, Hydrogen from catalytic reforming of biomass-derived hydrocarbons in liquid water, Nature 418 (2002) 964–967, http://dx.doi.org/10.1038/nature01009.

[34] R.L. Manfro, A.F. da Costa, N.F.P. Ribeiro, M.M.V.M. Souza, Hydrogen production by aqueous-phase reforming of glycerol over nickel catalysts supported on CeO_2, Fuel Process. Technol. 92 (2011) 330–335, http://dx.doi.org/10.1016/j.fuproc.2010.09.024.

[35] A.O. Menezes, M.T. Rodrigues, A. Zimmaro, L.E.P. Borges, M.A. Fraga, Production of renewable hydrogen from aqueous-phase reforming of glycerol over Pt catalysts supported on different oxides, Renew. Energy 36 (2011) 595–599, http://dx.doi.org/10.1016/j.renene.2010.08.004.

[36] P.V. Tuza, R.L. Manfro, N.F.P. Ribeiro, M.M.V.M. Souza, Production of renewable hydrogen by aqueous-phase reforming of glycerol over Ni–Cu catalysts derived from hydrotalcite precursors, Renew. Energy 50 (2013) 408–414, http://dx.doi.org/10.1016/j.renene.2012.07.006.

[37] A.J. Byrd, K.K. Pant, R.B. Gupta, Hydrogen production from glycerol by reforming in supercritical water over Ru/Al_2O_3 catalyst, Fuel 87 (2008) 2956–2960, http://dx.doi.org/10.1016/j.fuel.2008.04.024.

[38] F.J. Gutiérrez Ortiz, A. Serrera, S. Galera, P. Ollero, Experimental study of the supercritical water reforming of glycerol without the addition of a catalyst, Energy 56 (2013) 193–206, http://dx.doi.org/10.1016/j.energy.2013.04.046.

[39] T. Pairojpiriyakul, E. Croiset, W. Kiatkittipong, K. Kiatkittipong, A. Arpornwichanop, S. Assabumrungrat, Hydrogen production from catalytic supercritical water reforming of glycerol with cobalt-based catalysts, Int. J. Hydrog. Energy 38 (2013) 4368–4379, http://dx.doi.org/10.1016/j.ijhydene.2013.01.169.

[40] Y.C. Lin, Catalytic valorization of glycerol to hydrogen and syngas, Int. J. Hydrog. Energy 38 (2013) 2678–2700, http://dx.doi.org/10.1016/j.ijhydene.2012.12.079.

[41] B. Dou, Y. Song, C. Wang, H. Chen, Y. Xu, Hydrogen production from catalytic steam reforming of biodiesel byproduct glycerol: issues and challenges, Renew. Sust. Energy Rev. 30 (2014) 950–960, http://dx.doi.org/10.1016/j.rser.2013.11.029.

[42] L.F. Bobadilla, A. Penkova, F. Romero-Sarria, M.A. Centeno, J.A. Odriozola, Influence of the acid-base properties over NiSn/MgO–Al_2O_3 catalysts in the hydrogen production from glycerol steam reforming, Int. J. Hydrog. Energy 39 (2014) 5704–5712, http://dx.doi.org/10.1016/j.ijhydene.2014.01.136.

[43] C.A. Franchini, W. Aranzaez, A.M.D. de Farias, G. Pecchi, M.A. Fraga, Ce-substituted $LaNiO_3$ mixed oxides as catalyst precursors for glycerol steam reforming, Appl. Catal. B Environ. 147 (2014) 193–202, http://dx.doi.org/10.1016/j.apcatb.2013.08.036.

[44] H. Chen, Y. Ding, N.T. Cong, B. Dou, V. Dupont, M. Ghadiri, P.T. Williams, A comparative study on hydrogen production from steam-glycerol reforming: thermodynamics and experimental, Renew. Energy 36 (2011) 779–788, http://dx.doi.org/10.1016/j.renene.2010.07.026.

[45] X. Wang, S. Li, H. Wang, B. Liu, X. Ma, Thermodynamic analysis of glycerin steam reforming, Energy Fuel 22 (2008) 4285–4291, http://dx.doi.org/10.1016/j.jpowsour.2014.09.093.

[46] S. Adhikari, S. Fernando, A. Haryanto, A comparative thermodynamic and experimental analysis on hydrogen production by steam reforming of glycerin, Energy Fuel 21 (2007) 2306–2310, http://dx.doi.org/10.1021/ef070035l.

[47] C.C.R.S. Rossi, C.G. Alsonso, O.A.C. Antunes, R. Guirardello, L. Cardozo-Filho, Thermodynamic analysis of steam reforming of ethanol and glycerine for hydrogen production, Int. J. Hydrog. Energy 34 (2009) 323–332, http://dx.doi.org/10.1016/j.ijhydene.2008.09.071.

[48] S. Adhikari, S. Fernando, S.R. Gwaltney, S.D. Filip To, R.M. Bricka, P.H. Steele, A. Haryanto, A thermodynamic analysis of hydrogen production by steam reforming of glycerol, Int. J. Hydrog. Energy 32 (2007) 2875–2880, http://dx.doi.org/10.1016/j.jpowsour.2014.09.093.

[49] M.E. Sad, H.A. Duarte, C.H. Vignatti, C.L. Padro, C.R. Apesteguıa, Steam reforming of glycerol: hydrogen production optimization, Int. J. Hydrog. Energy 40 (2015) 6097–6106, http://dx.doi.org/10.1016/j.ijhydene.2015.03.043.

[50] A.C.D. Freitas, R. Guirardello, Comparison of several glycerol reforming methods for hydrogen and syngas production using Gibbs energy minimization, Int. J. Hydrog. Energy 39 (2014) 17969–17984, http://dx.doi.org/10.1016/j.ijhydene.2014.03.130.

[51] F. Pompeo, G.F. Santori, N.N. Nichio, Hydrogen production by glycerol steam reforming with Pt/SiO_2 and Ni/SiO_2 catalysts, Catal. Today 172 (2011) 183–188, http://dx.doi.org/10.1016/j.cattod.2011.05.001.

[52] S.M. de Rezende, C.A. Franchini, M.L. Dieuzeide, A.M.D. de Farias, N. Amadeo, M.A. Fraga, Glycerol steam reforming over layered double hydroxide-supported Pt catalysts, Chem. Eng. J. 272 (2015) 108–118, http://dx.doi.org/10.1016/j.cej.2015.03.033.

[53] Z. Wei, A.M. Karim, Y. Li, D.L. King, Y. Wang, Elucidation of the roles of Re in steam reforming of glycerol over Pt-Re/C catalysts, J. Catal. 322 (2015) 49–59, http://dx.doi.org/10.1016/j.jcat.2014.11.006.

[54] F. Pompeo, G. Santori, N.N. Nichio, Hydrogen and/or syngas from steam reforming of glycerol. Study of platinum catalysts, Int. J. Hydrog. Energy 35 (2010) 8912–8920, http://dx.doi.org/10.1016/j.ijhydene.2010.06.011.

[55] R.R. Soares, D.A. Simonetti, J.A. Dumesic, Glycerol as a source for fuels and chemicals by low-temperature catalytic processing, Angew. Chem. Int. Ed. 45 (2006) 3982–3985, http://dx.doi.org/10.1002/anie.200600212.

[56] A. Gallo, C. Pirovano, P. Ferrini, M. Marelli, R. Psaro, S. Santangelo, G. Faggio, V. Dal Santo, Influence of reaction parameters on the activity of ruthenium based catalysts for glycerol steam reforming, Appl. Catal. B Environ. 121-122 (2012) 40–49, http://dx.doi.org/10.1016/j.apcatb.2012.03.013.

[57] J. Kim, D. Lee, Glycerol steam reforming on supported Ru-based catalysts for hydrogen production for fuel cells, Int. J. Hydrog. Energy 38 (2013) 11853–11862, http://dx.doi.org/10.1016/j.ijhydene.2013.06.141.

[58] T. Hirai, N.O. Ikenaga, T. Miyake, T. Suzuki, Production of hydrogen by steam reforming of glycerin on ruthenium catalyst, Energy Fuel 19 (2005) 1761–1762, http://dx.doi.org/10.1021/ef050121q.

[59] V. Chiodo, S. Freni, A. Galvagno, N. Mondello, F. Frusteri, Catalytic features of Rh and Ni supported catalysts in the steam reforming of glycerol to produce hydrogen, Appl. Catal. A Gen. 381 (2010) 1–7, http://dx.doi.org/10.1016/j.apcata.2010.03.039.

[60] B. Zhang, X. Tang, Y. Li, Y. Xu, W. She, Hydrogen production from steam reforming of ethanol and glycerol over ceria-supported metal catalysts, Int. J. Hydrog. Energy 32 (2007) 2367–2373, http://dx.doi.org/10.1016/j.ijhydene.2006.11.003.

[61] L.P.R. Profeti, E.A. Ticianelli, E.M. Assaf, Production of hydrogen via steam reforming of biofuels on Ni/CeO_2–Al_2O_3 catalysts promoted by noble metals, Int. J. Hydrog. Energy 34 (2009) 5049–5060, http://dx.doi.org/10.1016/j.ijhydene.2009.03.050.

[62] M. Araque, T.L.M. Martínez, J.C. Vargas, A.C. Roger, Hydrogen production by glycerol steam reforming over CeZrCo fluorite type oxides, Catal. Today 176 (2011) 352–356, http://dx.doi.org/10.1016/j.cattod.2010.11.066.

[63] T.L.M. Martínez, M. Araque, J.C. Vargas, A.C. Roger, Effect of Ce/Zr ratio in CeZr–CoRh catalysts on the hydrogen production by glycerol steam reforming, Appl. Catal. B Environ. 132–133 (2013) 499–510, http://dx.doi.org/10.1016/j.apcatb.2012.12.027.

[64] M. Araque, T.L.M. Martínez, J.C. Vargas, M.A. Centeno, A.C. Roger, Effect of the active metals on the selective H_2 production in glycerol steam reforming, Appl. Catal. B Environ. 125 (2012) 556–566, http://dx.doi.org/10.1016/j.apcatb.2012.06.028.

[65] V.V. Thyssen, T.A. Maia, E.M. Assaf, Ni supported on La_2O_3–SiO_2 used to catalyze glycerol steam reforming, Fuel 105 (2013) 358–363, http://dx.doi.org/10.1016/j.fuel.2012.06.105.

[66] S. Adhikari, S. Fernando, A. Haryanto, Hydrogen production from glycerin by steam reforming over nickel catalysts, Renew. Energy 33 (2008) 1097–1100, http://dx.doi.org/10.1016/j.renene.2007.09.005.

[67] C.D. Dave, K.K. Pant, Renewable hydrogen generation by steam reforming of glycerol over zirconia promoted ceria supported catalyst, Renew. Energy 36 (2011) 3195–3202, http://dx.doi.org/10.1016/j.renene.2011.03.013.

[68] M.L. Dieuzeide, M. Jobbagy, N. Amadeo, Glycerol steam reforming over Ni/γ-Al_2O_3 catalysts, modified with Mg (II). Effect of Mg (II) content, Catal. Today 213 (2013) 50–57, http://dx.doi.org/10.1016/j.cattod.2013.02.015.

[69] A. Ebshish, Z. Yaakob, B. Narayanan, A. Bshish, W.R.W. Daud, Steam reforming of glycerol over Ni supported alumina xerogel for hydrogen production, Energy Procedia 19 (2012) 552–559, http://dx.doi.org/10.1016/j.egypro.2012.05.067.

[70] E. Gallegos-Suárez, A. Guerrero-Ruiz, M. Fernández-García, I. Rodríguez-Ramos, A. Kubacka, Efficient and stable Ni-Ce glycerol reforming catalysts: chemical imaging

using X-ray electron and scanning transmission microscopy, Appl. Catal. B Environ. 165 (2015) 139–148, http://dx.doi.org/10.1016/j.apcatb.2014.10.007.

[71] A. Iriondo, J.F. Cambra, M.B. Guemez, V.L. Barrio, J. Requies, M.C. Sanchez-Sanchez, R.M. Navarro, Effect of ZrO_2 addition on Ni/Al_2O_3 catalyst to produce H_2 from glycerol, Int. J. Hydrog. Energy 37 (2012) 7084–7093, http://dx.doi.org/10.1016/j.ijhydene.2011.11.075.

[72] V. Nichele, M. Signoretto, F. Menegazzo, A. Gallo, V.D. Santo, G. Cruciani, G. Cerrato, Glycerol steam reforming for hydrogen production: design of Ni supported catalysts, Appl. Catal. B Environ. 111–112 (2012) 225–232, http://dx.doi.org/10.1016/j.apcatb.2011.10.003.

[73] E.A. Sanchez, R.A. Comelli, Hydrogen by glycerol steam reforming on a nickel–alumina catalyst: deactivation processes and regeneration, Int. J. Hydrog. Energy 37 (2012) 14740–14746, http://dx.doi.org/10.1016/j.ijhydene.2011.12.088.

[74] E.A. Sanchez, R.A. Comelli, Hydrogen production by glycerol steam-reforming over nickel and nickel–cobalt impregnated on alumina, Int. J. Hydrog. Energy 39 (2014) 8650–8655, http://dx.doi.org/10.1016/j.ijhydene.2013.12.067.

[75] S. Shao, A.W. Shi, C.L. Liu, R.Z. Yang, W.S. Dong, Hydrogen production from steam reforming of glycerol over Ni/CeZrO catalysts, Fuel Process. Technol. 125 (2014) 1–7, http://dx.doi.org/10.1016/j.fuproc.2014.03.022.

[76] L.F. Bobadilla, A. Penkova, A. Álvarez, M.I. Domínguez, F. Romero-Sarria, M.A. Centeno, J.A. Odriozola, Glycerol steam reforming on bimetallic $NiSn/CeO_2$–MgO–Al_2O_3 catalysts: influence of the support, reaction parameters and deactivation/ regeneration processes, Appl. Catal. A Gen. 492 (2015) 38–47, http://dx.doi.org/10.1016/j.apcata.2014.12.029.

[77] B. Dou, C. Wang, Y. Song, H. Chen, Y. Xu, Activity of Ni–Cu–Al based catalyst for renewable hydrogen production from steam reforming of glycerol, Energy Convers. Manag. 78 (2014) 253–259, http://dx.doi.org/10.1016/j.enconman.2013.10.067.

[78] M.A. Goula, A.A. Lemonidou, A.M. Efstathiou, Characterization of carbonaceous species formed during reforming of CH_4 with CO_2 over Ni/CaO–Al_2O_3 catalysts studied by various transient techniques, J. Catal. 161 (1996) 626–640, http://dx.doi.org/10.1006/jcat.1996.0225.

[79] K.K. Pant, R. Jain, S. Jain, Renewable hydrogen production by steam reforming of glycerol over Ni/CeO_2 catalyst prepared by precipitation deposition method, Korean J. Chem. Eng. 28 (2011) 1859–1866, http://dx.doi.org/10.1007/s11814-011-0059-8.

[80] A. Iriondo, V.L. Barrio, J.F. Cambra, P.L. Arias, M.B. Güemez, M.C. Sanchez-Sanchez, R.M. Navarro, J.L.G. Fierro, Glycerol steam reforming over Ni catalysts supported on ceria and ceria-promoted alumina, Int. J. Hydrog. Energy 35 (2010) 11622–11633, http://dx.doi.org/10.1016/j.ijhydene.2010.05.105.

[81] M.L. Dieuzeide, V. Iannibelli, M. Jobbagy, N. Amadeo, Steam reforming of glycerol over Ni/Mg/γ-Al_2O_3 catalysts. Effect of calcination temperatures, Int. J. Hydrog. Energy 37 (2012) 14926–14930, http://dx.doi.org/10.1016/j.ijhydene.2011.12.086.

[82] Y.J. Go, G.S. Go, H.J. Lee, D.J. Moon, N.C. Park, Y.C. Kim, The relation between carbon deposition and hydrogen production in glycerol steam reforming, Int. J. Hydrog. Energy 40 (2015) 11840–11847, http://dx.doi.org/10.1016/j.ijhydene.2015.06.100.

[83] S. Ramesh, E.H. Yang, J.S. Jung, D.J. Moon, Copper decorated perovskite an efficient catalyst for low temperature hydrogen production by steam reforming of glycerol, Int. J. Hydrog. Energy (2015) 11428–11435, http://dx.doi.org/10.1016/j.ijhydene.2015.02.013.

[84] C. Wang, B. Dou, H. Chen, Y. Song, Y. Xu, X. Du, T. Luo, C. Tan, Hydrogen production from steam reforming of glycerol by Ni–Mg–Al based catalysts in a fixed-bed reactor, Chem. Eng. J. 220 (2013) 133–142, http://dx.doi.org/10.1016/j.cej.2013.01.050.

[85] Z.Y. Huang, C.H. Xu, J. Meng, C.F. Zheng, H.W. Xiao, J. Chen, Y.X. Zhang, Glycerol steam reforming to syngas over Ni-based catalysts on commercial Linde-type 5A zeolite modified by metal oxides, J. Environ. Chem. Eng. 2 (2014) 598–604, http://dx.doi.org/10.1016/j.jece.2013.10.015.

[86] S. Adhikari, S.D. Fernando, S.D.F. To, R.M. Bricka, R.H. Steele, A. Haryanto, Conversion of glycerol to hydrogen via a steam reforming process over nickel catalysts, Energy Fuel 22 (2008) 1220–1226, http://dx.doi.org/10.1021/ef700520f.

[87] M.L. Dieuzeide, M. Jobbagy, N. Amadeo, Glycerol steam reforming over Ni/mg/γ-Al_2O_3 catalysts effect of Ni(II) content, Int. J. Hydrog. Energy 39 (2014) 16976–16982, http://dx.doi.org/10.1016/j.ijhydene.2014.08.097.

[88] S.H. Kim, J.S. Jung, E.H. Yang, K.Y. Lee, D.J. Moon, Hydrogen production by steam reforming of biomass-derived glycerol over Ni-based catalysts, Catal. Today 228 (2014) 145–151, http://dx.doi.org/10.1016/j.cattod.2013.11.043.

[89] G. Wu, S. Li, C. Zhang, T. Wang, J. Gong, Glycerol steam reforming over perovskite-derived nickel-based catalysts, Appl. Catal. B Environ. 144 (2014) 277–285, http://dx.doi.org/10.1016/j.apcatb.2013.07.028.

[90] J.A. Calles, A. Carrero, A.J. Vizcaíno, L. García-Moreno, Hydrogen production by glycerol steam reforming over SBA-15-supported nickel catalysts: effect of alkaline earth promoters on activity and stability, Catal. Today 227 (2014) 198–206, http://dx.doi.org/10.1016/j.cattod.2013.11.006.

[91] C.K. Cheng, S.Y. Foo, A.A. Adesina, Carbon deposition on bimetallic Co–Ni/Al_2O_3 catalyst during steam reforming of glycerol, Catal. Today 164 (2011) 268–274, http://dx.doi.org/10.1016/j.cattod.2010.10.040.

[92] A.A. Schwengber, H.J. Alves, R.A. Schaffner, F.A. da Silva, R. Sequinel, V.R. Bach, R.J. Ferracin, Overview of glycerol reforming for hydrogen production, Renew. Sust. Energ. Rev. 58 (2016) 259–266, http://dx.doi.org/10.1016/j.rser.2015.12.279.

[93] A. Iriondo, V.L. Barrio, J.F. Cambra, P.L. Arias, M.B. Gúemez, R.M. Navarro, M.C. Sánchez-Sánchez, J.L.G. Fierro, Hydrogen production from glycerol over nickel catalysts supported on Al_2O_3 modified by Mg, Zr, Ce or La, Top. Catal. 49 (2008) 46–58, http://dx.doi.org/10.1007/s11244-008-9060-9.

[94] E.A. Sanchez, M.A. D'Angelo, R.A. Comelli, Hydrogen production from glycerol on Ni/Al_2O_3 catalyst, Int. J. Hydrog. Energy 35 (2010) 5902–5907, http://dx.doi.org/10.1016/j.ijhydene.2009.12.115.

[95] C.K. Cheng, S.Y. Foo, A.A. Adesina, H_2-rich synthesis gas production over Co/Al_2O_3 catalyst via glycerol steam reforming, Catal. Commun. 12 (2010) 292–298, http://dx.doi.org/10.1016/j.catcom.2010.09.018.

[96] M.A. Goula, N.D. Charisiou, K.N. Papageridis, A. Delimitis, E. Pachatouridou, E.F. Iliopoulou, Nickel on alumina catalysts for the production of hydrogen rich mixtures via the biogas dry reforming reaction: influence of the synthesis method, Int. J. Hydrog. Energy 40 (2015) 9183–9200, http://dx.doi.org/10.1016/j.ijhydene.2015.05.129.

[97] M.A. Goula, O.A. Bereketidou, K.N. Papageridis, N.D. Charisiou, Influence of the preparation procedure parameters on the performance of Ni/γ-alumina catalysts for the biogas reforming reaction, Proc. Int. Conf. WHEC 1435–1441 (2014).

[98] A.A. Lemonidou, M.A. Goula, I.A. Vasalos, Carbon dioxide reforming of methane over 5 wt% nickel calcium aluminate catalysts - effect of preparation method, Catal. Today 46 (1998) 175–183, http://dx.doi.org/10.1016/S0920-5861(98)00339-3.

[99] M. Ni, D.Y.C. Leung, M.K.H. Leung, A review on reforming bio-ethanol for hydrogen production, Int. J. Hydrog. Energy 32 (2007) 3238–3247, http://dx.doi.org/10.1016/j.ijhydene.2007.04.038.

[100] J.G. Seo, M.H. Youn, S. Park, J.S. Chung, I.K. Song, Hydrogen production by steam reforming of liquefied natural gas (LNG) over Ni/Al_2O_3–ZrO_2 xerogel catalysts: effect of calcination temperature of Al_2O_3–ZrO_2 xerogel supports, Int. J. Hydrog. Energy 34 (2009) 3755–3763, http://dx.doi.org/10.1016/j.ijhydene.2009.03.030.

[101] E. Kordouli, V. Dracopoulos, T. Vaimakis, K. Bourikas, A. Lycourghiotis, C. Kordulis, Comparative study of phase transition and textural changes upon calcination of two commercial titania samples: a pure anatase and a mixed anatase-rutile, J. Solid State Chem. 232 (2015) 42–49, http://dx.doi.org/10.1016/j.jssc.2015.08.040.

[102] S.S. Akarmazyan, P. Panagiotopoulou, A. Kambolis, C. Papadopoulou, D.I. Kondarides, Methanol dehydration to dimethylether over Al_2O_3 catalysts, Appl. Catal. B 145 (2014) 136–148, http://dx.doi.org/10.1016/j.apcatb.2012.11.043.

[103] I.V. Yentekakis, G. Goula, P. Panagiotopoulou, S. Kampouri, M.J. Taylor, G. Kyriakou, R.M. Lambert, Stabilization of catalyst particles against sintering on oxide supports with high oxygen ion lability exemplified by Ir-catalyzed decomposition of N_2O, Appl. Catal. B 192 (2016) 357–364, http://dx.doi.org/10.1016/j.apcatb.2016.04.011.

[104] K. Kousi, N. Chourdakis, H. Matralis, D. Kondarides, C. Papadopoulou, X. Verykios, Glycerol steam reforming over modified Ni-based catalysts, Appl. Catal. A Gen. 518 (2016) 129–141, http://dx.doi.org/10.1016/j.apcata.2015.11.047.

[105] N.D. Charisiou, G. Siakavelas, K.N. Papageridis, A. Baklavaridis, L. Tzounis, D.G. Avraam, M.A. Goula, Syngas production via the biogas dry reforming reaction over nickel supported on modified with CeO_2 and/or La_2O_3 alumina catalysts, J. Nat. Gas Sci. Eng. 31 (2016) 164–183, http://dx.doi.org/10.1016/j.jngse.2016.02.021.

[106] O.A. Bereketidou, M.A. Goula, Biogas reforming for syngas production over nickel supported on ceria-alumina catalysts, Catal. Today 195 (2012) 93–100, http://dx.doi.org/10.1016/j.cattod.2012.07.006.

[107] W.J. Zhou, B. Zhou, W.Z. Li, Z.H. Zhou, S.Q. Song, G.Q. Sun, Q. Xin, S. Douvartzides, M. Goula, P. Tsiakaras, Performance comparison of low-temperature direct alcohol fuel cells with different anode catalysts, J. Power Sources 126 (2004) 16–22, http://dx.doi.org/10.1016/j.jpowsour.2003.08.009.

[108] Z. Boukha, C. Jiménez-González, B. de Rivas, J.R. González-Velasco, J.I. Gutiérrez-Ortiz, R. López-Fonseca, Synthesis, characterisation and performance evaluation of spinel-derived Ni/Al_2O_3 catalysts for various methane reforming reactions, Appl. Catal. B Environ. 158–159 (2014) 190–201, http://dx.doi.org/10.1016/j.apcatb.2014.04.014.

[109] C. Jiménez-González, Z. Boukha, B. de Rivas, J.J. Delgado, M.A. Cauqui, J.R. González-Velasco, J.I. Gutiérrez-Ortiz, R. López-Fonseca, Structural characterisation of Ni/alumina reforming catalysts activated at high temperatures, Appl. Catal. A Gen. 466 (2013) 9–20, http://dx.doi.org/10.1016/j.apcata.2013.06.017.

[110] G. Li, L. Hu, J.M. Hill, Comparison of reducibility and stability of alumina-supported Ni catalysts prepared by impregnation and co-precipitation, Appl. Catal. A Gen. 301 (2006) 16–24, http://dx.doi.org/10.1016/j.apcata.2005.11.013.

[111] H.S. Roh, K.W. Jun, S.E. Park, Methane-reforming reactions over Ni/Ce–ZrO_2/θ-Al_2O_3 catalysts, Appl. Catal. A Gen. 251 (2003) 275–283, http://dx.doi.org/10.1016/S0926-860X(03)00359-4.

[112] P. Kim, Y. Kim, H. Kim, I.K. Song, K. Yi, Synthesis and characterization of mesoporous alumina with nickel incorporated for use in the partial oxidation of methane into synthesis gas, Appl. Catal. A Gen. 272 (2004) 157–166, http://dx.doi.org/10.1016/j.apcata.2004.05.055.

[113] H.A. Oliveira, D.F. Franceschini, F.B. Passos, Cobalt catalyst characterization for methane decomposition and carbon nanotube growth, J. Braz. Chem. Soc. 25 (2014) 2339–2349, http://dx.doi.org/10.5935/0103-5053.20140243.

[114] B. Jongsomjit, J. Panpranot, J.G. Goodwin Jr., Co-support compound formation in alumina-supported cobalt catalysts, J. Catal. 204 (2001) 98–109, http://dx.doi.org/10.1006/jcat.2001.3387.

[115] J. Llorca, J.A. Dalmon, P.R. de la Piscina, N. Homs, In situ magnetic characterisation of supported cobalt catalysts under steam reforming of ethanol, Appl. Catal. A Gen. 243 (2003) 261–269, http://dx.doi.org/10.1016/S0926-860X(02)00546-X.

[116] J. Llorca, P.R. de la Piscina, J.A. Dalmon, N. Homs, Transformation of Co_3O_4 during ethanol steam-re-forming. Activation process for hydrogen production, Chem. Mater. 16 (2004) 3573–3578, http://dx.doi.org/10.1021/cm049311p.

[117] C. He, M. Paulus, W. Chu, J. Find, J.A. Nickl, K. Köhler, Selective catalytic reduction of NO by C_3H_8 over $CoOx/Al_2O_3$: an investigation of structure–activity relationships, Catal. Today 131 (2008) 305–313, http://dx.doi.org/10.1016/j.cattod.2007.10.024.

[118] L. Zhang, L. Dong, W. Yu, L. Liu, Y. Deng, B. Liu, H. Wan, F. Gao, K. Sun, L. Dong, Effect of cobalt precursors on the dispersion, reduction, and CO oxidation of CoOx/γ-Al_2O_3 catalysts calcined in N_2, J. Colloid Interface Sci. 355 (2011) 464–471, http://dx.doi.org/10.1016/j.jcis.2010.11.076.

[119] G. Derrien, C. Charnay, J. Zajac, D.J. Jones, J. Rozière, Copper-containing monodisperse mesoporous silica nanospheres by a smart one-step approach, Chem. Commun. (2008) 3118–3120, http://dx.doi.org/10.1039/B804593C.

[120] B. Putrakumar, N. Nagaraju, V.P. Kumar, K.V.R. Chary, Hydrogenation of levulinic acid to γ-valerolactone over copper catalysts supported on γ-Al_2O_3, Catal. Today 250 (2015) 209–217, http://dx.doi.org/10.1016/j.cat.2014.07.014.

[121] R. Yang, X. Li, J. Wu, X. Zhang, Z. Zhang, Y. Cheng, et al., Hydrotreating of crude 2-ethylhexanol over Ni/Al_2O_3 catalysts: surface Ni species-catalytic activity correlation, Appl. Catal. A Gen. 368 (2009) 105–112, http://dx.doi.org/10.1016/j.apcata.2009.08.021.

[122] R.C.M.S. Rosenir, A.O. Hugo, C.P.F.A. Guarino, B.B. Toledo, M.B.T. Moura, B.T.M. Oliveira, F.B. Passos, Effect of support on methane decomposition for hydrogen production over cobalt catalysts, Int. J. Hydrog. Energy 41 (2016) 6763–6772, http://dx.doi.org/10.1016/j.ijhydene.2016.02.101.

[123] S. Storsaeter, B. Totdal, J.C. Walmsley, B.S. Tanem, A. Holmen, Characterization of alumina-, silica-, and titania-supported cobalt Fischer-Tropsch catalysts, J. Catal. 236 (2005) 139–236, http://dx.doi.org/10.1016/j.cat.2005.09.021.

[124] W.P. Dow, Y.P. Wang, T.J. Huang, TPR and XRD studies of yttria-doped ceria/alumina-supported copper oxide catalyst, Appl. Catal. A Gen. 190 (2000) 25–34, http://dx.doi.org/10.1016/S0926-860X(99)00286-0.

[125] A. Patel, P. Shukl, J. Chen, T.E. Rufford, S. Wang, V. Rudolph, Z. Zhu, Structural sensitivity of mesoporous alumina for copper catalyst loading used for NO reduction in presence of CO, Chem. Eng. Res. Des. 101 (2015) 27–43, http://dx.doi.org/10.1016/j.cherd.2015.03.027.

[126] Z.H. Zhu, H.Y. Zhu, S.B. Wang, G.Q. Lu, Preparation and characterization of copper catalysts supported on mesoporous Al_2O_3 nanofibers for N_2O reduction to N_2, Catal. Lett. 91 (2003) 73–81, http://dx.doi.org/10.1023/B:CATL.0000006320.85524.f1.

[127] R. Bechara, A. Aboukaïs, B. J.-P, X-ray photoelectron spectroscopic study of a Cu–Al–O catalyst under H_2 or CO atmospheres, J. Chem. Soc. Faraday Trans. 89 (1993) 1257–1262, http://dx.doi.org/10.1039/FT9938901257.

[128] M.A. Goula, S.K. Kontou, P.E. Tsiakaras, Hydrogen production by ethanol steam reforming over a commercial Pd/γ-Al_2O_3 catalyst, App. Catal. B Environ. 49 (2004) 135–144, http://dx.doi.org/10.1016/j.apcatb.2003.12.001.

[129] M.A. Goula, S. Kontou, W. Zhou, X. Qin, P.E. Tsiakaras, Hydrogen production over a commercial Pd/Al_2O_3 catalyst for fuel cell utilization, Ionics 9 (2003) 248–252, http://dx.doi.org/10.1007/BF02375975.

[130] X. Wang, M. Li, S. Li, H. Wang, S. Wang, X. Ma, Hydrogen production by glycerol steam reforming with/without calcium oxide sorbent: a comparative study of thermodynamic and experimental work, Fuel Process. Technol. 91 (2010) 1812–1818, http://dx.doi.org/10.1016/j.fuproc.2010.08.003.

[131] B.L. Dou, V. Dupont, P.T. Williams, H.S. Chen, Y.L. Ding, Thermogravimetric kinetics of crude glycerol, Bioresour. Technol. 100 (2009) 2613–2620, http://dx.doi.org/10.1016/j.biortech.2008.11.037.

[132] G. Wu, C. Zhang, S. Li, Z. Han, T. Wang, X. Ma, J. Gong, Hydrogen production via glycerol steam reforming over Ni/Al_2O_3: influence of nickel precursors, ACS Sustain. Chem. Eng. 1 (2013) 1052–1062, http://dx.doi.org/10.1021/sc400123f.

[133] F. Frusteri, S. Freni, L. Spadaro, V. Chiodo, G. Bonura, S. Donato, S. Cavallaro, H_2 production for MC fuel cell by steam reforming of ethanol over MgO supported Pd, Rh, Ni and Co catalysts, Catal. Commun. 5 (2004) 611–615, http://dx.doi.org/10.1016/j.catcom.2004.07.015.

[134] J. Llorca, N. Homs, J. Sales, J.L.G. Fierro, P.R. de la Piscina, Effect of sodium addition on the performance of Co–ZnO-based catalysts for hydrogen production from bioethanol, J. Catal. 222 (2004) 470–480, http://dx.doi.org/10.1016/j.jcat.2003.12.008.

[135] M.S. Batista, R.K.S. Santos, E.M. Assaf, J.M. Assaf, E.A. Ticianelli, High efficiency steam reforming of ethanol by cobalt-based catalysts, J. Power Sources 134 (2004) 27–32, http://dx.doi.org/10.1016/j.jpowsour.2004.01.052.

[136] C.K. Cheng, S.Y. Foo, A.A. Adesina, Glycerol steam reforming over bimetallic CoNi/Al_2O_3, Ind. Eng. Chem. Res. 49 (2010) 10804–10817, http://dx.doi.org/10.1021/ie100462t.

[137] A. Casanovas, M. Roig, C. de Leitenburg, A. Trovatelli, J. Llorca, Ethanol steam reforming and water gas shift over Co/ZnO catalytic honeycombs doped with Fe, Ni, Cu, Cr and Na, Int. J. Hydrog. Energy 35 (2010) 7690–7698, http://dx.doi.org/10.1016/j.ijhydene.2010.05.099.

[138] A. Carrero, J.A. Calles, A.J. Vizcaıno, Effect of Mg and Ca addition on coke deposition over Cu–Ni/SiO_2 catalysts for ethanol steam reforming, Chem. Eng. J. 163 (2010) 395–402, http://dx.doi.org/10.1016/j.cej.2010.07.029.

[139] F. Marino, G. Baronetti, M. Jobbagy, M. Laborde, Cu–Ni–K/g-Al_2O_3 supported catalysts for ethanol steam reforming: formation of hydrotalcite-type compounds as a result of metal-support interaction, Appl. Catal. A Gen. 238 (2003) 41–54, http://dx.doi.org/10.1016/S0926-860X(02)00113-8.

[140] F. Wang, Y. Li, W. Cai, E. Zhan, X. Mu, W. Shen, Ethanol steam reforming over Ni and Ni–Cu catalysts, Catal. Today 146 (2009) 31–36, http://dx.doi.org/10.1016/j.apcata.2007.04.030.

[141] L.C. Chen, S.D. Lin, The ethanol steam reforming over Cu–Ni/SiO_2 catalysts: effect of Cu/Ni ratio, Appl. Catal. B Environ. 106 (2011) 639–649, http://dx.doi.org/10.1016/j.apcatb.2011.06.028.

[142] E. Finocchio, I. Rossetti, G. Ramis, Redox properties of Co- and Cu-based catalysts for the steam reforming of ethanol, Int. J. Hydrog. Energy 38 (2013) 3213–3225, http://dx.doi.org/10.1016/j.ijhydene.2012.12.137.

[143] B.C. Miranda, R.J. Chimentão, J. Szanyi, A.H. Braga, J.B.O. Santos, F. Gispert-Guirado, J. Llorca, F. Medina, Influence of copper on nickel-based catalysts in the conversion of glycerol, App. Catal. B Environ. 166-167 (2015) 166–180, http://dx.doi.org/10.1016/j.apcatb.2014.11.019.

[144] B.C. Miranda, R.J. Chimentão, J.B.O. Santos, F. Gispert-Guirado, J. Llorca, F. Medina, F. López Bonillo, J.E. Sueiras, Conversion of glycerol over 10%Ni/γ-Al_2O_3 catalyst, Appl. Catal. B Environ. 147 (2014) 464–480, http://dx.doi.org/10.1016/j.apcatb.2013.09.026.

[145] S. Sato, M. Akiyama, R. Takahashi, T. Hara, K. Inui, M. Yokota, Vapor-phase reaction of polyols over copper catalysts, Appl. Catal. A Gen. 347 (2008) 186–191, http://dx.doi.org/10.1016/j.apcata.2008.06.013.

[146] N. Palmeri, V. Chiodo, S. Freni, F. Frusteri, J.C.J. Bart, S. Cavallaro, Hydrogen from oxygenated solvents by steam reforming on Ni/Al_2O_3 catalyst, Int. J. Hydrog. Energy 33 (2008) 6627–6634, http://dx.doi.org/10.1016/j.ijhydene.2008.07.064.

[147] S. Cavallaro, V. Chiodo, S. Freni, N. Mondello, F. Frusteri, Performance of Rh/Al_2O_3 catalyst in the steam reforming of ethanol: H_2 production for MCFC, Appl. Catal. A Gen. 249 (2003) 119–128, http://dx.doi.org/10.1016/S0926-860X(03)00189-3.

[148] C.H. Bartholomew, Carbon deposition in steam reforming and methanation, Catal. Rev. Sci. Eng. 24 (1982) 67–112, http://dx.doi.org/10.1080/03602458208079650.

[149] B. Dou, V. Dupont, G. Rickett, N. Blakeman, P. Williams, H. Chen, Hydrogen production by sorption-enhanced steam reforming of glycerol, Bioresour. Technol. 100 (2009) 3540–3547, http://dx.doi.org/10.1016/j.biortech.2009.02.036.

[150] S. Adhikari, S.D. Fernando, A. Haryanto, Hydrogen production from glycerol: an update, Energy Convers. Manag. 50 (2009) 2600–2604, http://dx.doi.org/10.1016/j.enconman.2009.06.011.

[151] A. Iriondo, M.B. Guemez, V.L. Barrio, J.F. Cambra, P.L. Arias, M.C. Sanchez-Sanchez, R.M. Navarro, J.L.G. Fierro, Glycerol conversion into H_2 by steam reforming over Ni and PtNi catalysts supported on MgO modified g-Al_2O_3, Stud. Surf. Sci. Catal. 175 (2010) 449–452, http://dx.doi.org/10.1016/S0167-2991(10)75082-5.

[152] A. Corma, G.H. Huber, L. Sauvanaud, P. O'Connor, Biomass to chemicals: catalytic conversion of glycerol/water mixtures into acrolein, reaction network, J. Catal. 257 (2008) 163–171, http://dx.doi.org/10.1016/j.jcat.2008.04.016.

[153] J.B. Paine III, Y.B. Pithawalla, J.D. Naworal, C.E. Thomas Jr., Carbohydrate pyrolysis mechanisms from isotopic labeling: part 1: the pyrolysis of glycerin: discovery of competing fragmentation mechanisms affording acetaldehyde and formaldehyde and the implications for carbohydrate pyrolysis, J. Anal. Appl. Pyrolysis 80 (2007) 297–311, http://dx.doi.org/10.1016/j.jaap.2007.03.007.

[154] W. Buhler, E. Dinjus, H.J. Ederer, A. Kruse, C. Mas, Ionic reactions and pyrolysis of glycerol as competing reaction pathways in near- and supercritical water, J. Supercrit. Fluids 22 (2002) 37–53, http://dx.doi.org/10.1016/S0896-8446(01)00105-X.

[155] S.H. Chai, H.P. Wang, Y. Liang, B.Q. Xu, Sustainable production of acrolein: gas-phase dehydration of glycerol over Nb_2O_5 catalyst, J. Catal. 250 (2007) 342–349, http://dx.doi.org/10.1016/j.jcat.2007.06.016.

[156] W. Suprun, M. Lutecki, T. Haber, H. Papp, Acidic catalysts for the dehydration of glycerol: activity and deactivation, J. Mol. Catal. A 309 (2009) 71–78, http://dx.doi.org/10.1016/j.molcata.2009.04.017.

[157] J. Barrault, J.M. Clacens, Y. Pouilloux, Selective oligomerization of glycerol over mesoporous catalysts, Top. Catal. 27 (2004) 137–142, http://dx.doi.org/10.1023/B:TOCA.0000013548.16699.1c.

[158] B. Katryniok, S. Paul, V. Bellière-Baca, P. Rey, F. Dumeignil, Glycerol dehydration to acrolein in the context of new uses of glycerol, Green Chem. 12 (2010) 2079–2098, http://dx.doi.org/10.1039/C0GC00307G.

[159] D. Hernandez, M. Velasquez, P. Ayrault, D. Lopez, J.J. Fernandez, A. Santamaria, C. Batiot-Dupeyrat, Gas phase glycerol conversion over lanthanum based catalysts: $LaNiO_3$ and La_2O_3, Appl. Catal. A Gen. 467 (2013) 315–324.

[160] D. Stosic, S. Bennici, S. Sirotin, C. Calais, J.L. Couturier, J.L. Dubois, A. Travert, A. Auroux, Glycerol dehydration over calcium phosphate catalysts: effect of acidic-basic features on catalytic performance, Appl. Catal. A Gen. 447-448 (2012) 124–134, http://dx.doi.org/10.1016/j.apcata.2012.09.029.

[161] E. Tsukuda, S. Sato, R. Takahashi, T. Sodesawa, Production of acrolein from glycerol over silica-supported heteropoly acids, Catal. Commun. 8 (2007) 1349–1353, http://dx.doi.org/10.1016/j.catcom.2006.12.006.

[162] K. Pathak, K.M. Reddy, N.N. Bakhshi, A.K. Dalai, Catalytic conversion of glycerol to value added liquid products, Appl. Catal. A 372 (2010) 224–238, http://dx.doi.org/10.1016/j.apcata.2009.10.036.

[163] P.S. Van Damme, S. Narayanan, G.F. Froment, Thermal cracking of propane and propane-propylene mixtures: pilot plant versus industrial data, AICHE J. 21 (1975) 1065–1073, http://dx.doi.org/10.1002/aic.690210604.

[164] Y.T. Shah, E.B. Stuart, K.D. Sheth, Coke formation during thermal cracking of n-octane, Ind. Eng. Chem. Process. Des. Dev. 15 (1976) 518, http://dx.doi.org/10.1021/i260060a007.

[165] K.M. Sundaram, G.F. Froment, Kinetics of coke deposition in the thermal cracking of propane, Chem. Eng. Sci. 34 (1979) 635–644, http://dx.doi.org/10.1016/0009-2509(79)85108-8.

[166] C.H. Bartholomew, M.V. Strasburg, H.Y. Hsieh, Effects of support on carbon formation and gasification on nickel during carbon monoxide hydrogenation, Appl. Catal. 36 (1988) 147, http://dx.doi.org/10.1016/S0166-9834(00)80111-6.

[167] J. Gascón, C. Téllez, J. Herguido, M. Menéndez, Propane dehydrogenation over a Cr_2O_3/Al_2O_3 catalyst: transient kinetic modelling of propene and coke formation, Appl. Catal. A Gen. 248 (2003) 105–116, http://dx.doi.org/10.1016/S0926-860X(03)00128-5.

[168] A.N. Fatsikostas, D.I. Kondarides, X.E. Verykios, Production of hydrogen for fuel cells by reformation of biomass-derived ethanol, Catal. Today 75 (2002) 145–155, http://dx.doi.org/10.1016/S0920-5861(02)00057-3.

[169] W.J. Cai, F.G. Wang, E.S. Zhan, A.C. Van Veen, C. Mirodatos, W.J. Shen, Hydrogen production from ethanol over Ir/CeO_2 catalysts: a comparative study of steam reforming, partial oxidation and oxidative steam reforming, J. Catal. 257 (2008) 96–107, http://dx.doi.org/10.1016/j.jcat.2008.04.009.

[170] Y. Cui, V. Galvita, L. Rihko-Struckmann, H. Lorenz, K. Sundmacher, Steam reforming of glycerol: the experimental activity of $La_{1-x}Ce_xNiO_3$ catalyst in comparison to the thermodynamic reaction equilibrium, Appl. Catal. B Environ. 90 (2009) 29–37, http://dx.doi.org/10.1016/j.apcatb.2009.02.006.

[171] O. Akdim, W.J. Cai, V. Fierro, H. Provendier, A. Van Veen, W.J. Shen, C. Mirodatos, Oxidative steam reforming of ethanol over Ni–Cu/SiO_2, Rh/Al_2O_3 and Ir/CeO_2: effect of metal and support on reaction mechanism, Top. Catal. 51 (2008) 22–38, http://dx.doi.org/10.1007/s11244-008-9122-z.

[172] E.B. Pereira, N. Homs, S. Marti, J.L.G. Fierro, P.R. de la Piscina, Oxidative steam-reforming of ethanol over Co/SiO_2, Co–Rh/SiO_2 and Co–Ru/SiO_2 catalysts: catalytic behavior and deactivation/regeneration processes, J. Catal. 257 (2008) 206–214, http://dx.doi.org/10.1016/j.jcat.2008.05.001.

[173] N. Srisiriwat, S. Therdthianwong, A. Therdthianwong, Oxidative steam reforming of ethanol over Ni/Al_2O_3 catalysts promoted by CeO_2, ZrO_2 and CeO_2–ZrO_2, Int. J. Hydrog. Energy 34 (2009) 2224–2234, http://dx.doi.org/10.1016/j.ijhydene.2008.12.058.

[174] G. Wen, Y. Xu, H. Ma, Z. Xu, Z. Tian, Production of hydrogen by aqueous-phase reforming of glycerol, Int. J. Hydrog. Energy 33 (2008) 6657–6666, http://dx.doi.org/10.1016/j.ijhydene.2008.07.072.

[175] B. Bayram, I.I. Soykal, D. von Deak, J.T. Miller, U.S. Ozkan, Ethanol steam reforming over Co-based catalysts: investigation of cobalt coordination environment under reaction conditions, J. Catal. 284 (2011) 77–89, http://dx.doi.org/10.1016/j.jcat.2011.09.001.

[176] D.J. Moodley, A.M. Saib, J.V.D. Loosdrecht, C.A. Welker-Nieuwoudt, B.H. Sigwe-bela, J.W. Niemantsverdriet, The impact of cobalt aluminate formation on the deactivation of cobalt-based Fischer-Tropsch synthesis catalysts, Catal. Today 171 (2011) 192–200, http://dx.doi.org/10.1016/j.cattod.2011.03.078.

[177] A.R. Passos, L. Martins, S.H. Pulcinelli, C.V. Santilli, V. Briois, Effect of the balance between Co(II) and Co(0) oxidation states on the catalytic activity of cobalt catalysts for ethanol steam reforming, Catal. Today 229 (2014) 88–94, http://dx.doi.org/10.1016/j.cattod.2013.10.080.

[178] A. Corma, P.J. Miguel, A.V. Orchilles, J. Catal, The role of reaction temperature and cracking catalyst characteristics in determining the relative rates of protolytic cracking, chain propagation, and hydrogen transfer, J. Catal. 145 (1994) 171–180, http://dx.doi.org/10.1006/jcat.1994.1020.

[179] F. Frusteri, S. Freni, V. Chiodo, L. Spadaro, O. di Blasi, G. Bonura, Steam reforming of bio-ethanol on alkali-doped Ni/MgO catalysts: hydrogen production for MC fuel cell, Appl. Catal. A Gen. 270 (2004) 1–7, http://dx.doi.org/10.1016/j.apcata.2004.03.052.